JOURNAL OF GEOPHYSICAL RESEARCH, VOL. 115, D07303, doi:10.1029/2009JD012714, 2010

Oxidant (O_3 + NO_2) production processes and formation regimes in Beijing

Keding Lu,[1] Yuanhang Zhang,[1] Hang Su,[1] Theo Brauers,[2] Charles C. Chou,[3] Andreas Hofzumahaus,[2] Shaw C. Liu,[3] Kazuyuki Kita,[4] Yutaka Kondo,[5] Min Shao,[1] Andreas Wahner,[2] Jialin Wang,[6] Xuesong Wang,[1] and Tong Zhu[1]

Received 23 June 2009; revised 17 November 2009; accepted 25 November 2009; published 8 April 2010.

[1] For CareBeijing-2006, two sites were established in urban and suburban regions of Beijing in summer 2006. Observations of O_3 and its precursors together with meteorological parameters at both sites are presented. Gross ozone production rate $P(O_3)$ and sensitivity to nitric oxides (NO_x) and volatile organic compounds (VOCs) were investigated using an observation-based photochemical box model (OBM). $P(O_3)$ varied from nearly zero to 120 and 50 ppb h^{-1} for urban and suburban sites, respectively. These rates were greater than the accumulation rates of the observed oxidant (O_3 + NO_2) concentrations. The O_3 episodes typically appeared under southerly wind conditions with high $P(O_3)$, especially at the urban site. Sensitivity studies with and without measured nitrous acid (HONO) as a model constraint suggested that the estimated $P(O_3)$ at both sites was strongly enhanced by radical production from HONO photolysis. Both NO_x- and VOC-sensitive chemistries existed over time scales from hours to days at the two sites. The variation in O_3-sensitive chemistry was relatively well explained by the ratio of the average daytime total VOC reactivity (k_{TVOC}) to NO, with the transition chemistry corresponding to a k_{TVOC}/NO value of 2–4 s^{-1} ppb^{-1}. Pronounced diurnal variations in the O_3 production regime were found. In the morning, conditions were always strongly VOC-limited, while in the afternoon, conditions were variable for different days and different sites. The model-calculated results were tested by measurements of H_2O_2, HNO_3, total OH reactivity, and HO_x radicals. The OBM was generally capable of correctly simulating the levels of $P(O_3)$, although it might tend to overpredict the VOC-sensitive chemistry.

Citation: Lu, K., et al. (2010), Oxidant (O_3 + NO_2) production processes and formation regimes in Beijing, *J. Geophys. Res.*, *115*, D07303, doi:10.1029/2009JD012714.

1. Introduction

[2] It has been well recognized that high surface ozone is mainly produced photochemically via sunlight-exposed reactions involving anthropogenic as well as biogenic nitrogen oxides (NO_x) and volatile organic compounds (VOCs). The photochemical ozone production rate $P(O_3)$ has a nonlinear dependence on the radical sources NO_x and VOCs. Moreover, this functional dependence, namely the $P(O_3)$-NO_x-VOC sensitivity, varies significantly under different photochemical conditions [*Sillman et al.*, 1990; *Kleinman et al.*, 1997; *Thornton et al.*, 2002]. Therefore, an effective reduction policy can only be achieved when the dependence of $P(O_3)$ on the precursors of O_3 is determined definitively. For that purpose, comprehensive field studies targeted at diagnosing the functional dependence under different photochemical regimes between O_3 and its precursors have been conducted in Europe, North America, and Japan [*Solomon et al.*, 2000]. Major insights gained from those field studies are as follows: (1) $P(O_3)$-NO_x-VOC sensitivity needs to be investigated individually in different regions because there is no geographically uniform response to NO_x and VOCs [*Hidy*, 2000]; (2) observation-based approaches developed in data interpretation of field studies are key complements of 3-D Eulerian model calculations [*Kleinman*, 2000]; and (3) generally, observation-based approaches involve certain simplifying assumptions that can result in artifacts in predicting either VOC- or NO_x-sensitive chemistry, and one needs to avoid or at least be aware of these potential problems [*Sillman*, 1999].

[1]College of Environmental Sciences and Engineering, Peking University, Beijing, China.
[2]Institute ICG-II: Troposphere, Forschungszentrum Juelich, Juelich, Germany.
[3]Research Center of Environment Change, Academia Sinica, Taipei, Taiwan.
[4]Faculty of Science, Ibaraki University, Mito, Japan.
[5]Research Center for Advanced Science and Technology, University of Tokyo, Tokyo, Japan.
[6]Department of Chemistry, National Central University, Chungli, Taiwan.

0148-0227/10/2009JD012714

[3] In the 1980s, air pollution in Chinese metropolitan areas (e.g., Beijing, Guangzhou, and Shanghai) was initially characterized as being London-type smog with SO_2 and sulfate as the major air pollutants [*Tang et al.*, 1990]. In the late 1990s, the air pollution shifted to a photochemical smog as evidenced by high concentrations of VOC, NO_x, and O_3 [*Zhang et al.*, 1998]. Recently, the term "air pollution complex" has been used to describe the severe air pollution caused by complex interactions between primary pollutants from direct emissions and secondary pollutants from atmospheric chemical-physical processes in both gaseous and aerosol phases [*Shao et al.*, 2006; *Zhang et al.*, 2008a].

[4] To examine the $P(O_3)$-NO_x-VOC sensitivity of the air pollution complex, two observation-based approaches, namely observation-based model (OBM) [*Cardelino and Chameides*, 1995] and photochemical age-based method [*Shiu et al.*, 2007], have recently been used in field campaigns at the Pearl River Delta (PRD) and in southern regions of Taiwan, respectively. Both the PRD and southern Taiwan regions were characterized by VOC-sensitive chemistry [*Shiu et al.*, 2007; *Zhang et al.*, 2007, 2008b]. According to the OBM, radical production from nitrous acid (HONO) and aldehyde photolysis contributed significantly to the $P(O_3)$, while high aerosol loading strongly suppressed $P(O_3)$ [*Zhang et al.*, 2007, 2008b]. As indicated by *Kanaya et al.* [2008], most of the work reviewed by *Sillman* [1999] implicitly assumed that the radicals (HO_x and RO_x) behaved according to the current tropospheric chemistry mechanism. This is also the case for previous OBM methods used in China. Obviously, this assumption is not necessarily valid for the air pollution complex in Chinese metropolitan regions. If the radicals do not behave as described by the mechanisms developed in Europe or North America, the $P(O_3)$ could be different from previous predictions. Furthermore, the VOC/NO_x ratios that result in the maximum production of ozone could also be different from the predictions. Therefore, tests of the chemical mechanisms that operate in the OBM based on direct measurements of radical concentrations or other directly measured parameters would be interesting and helpful.

[5] In recent years, the air quality in Beijing has become very poor; for example, the ambient air quality standard for ozone has frequently been exceeded [*Wang et al.*, 2006]. Many research activities were therefore planned and initiated aimed at the 2008 Summer Olympic Games as well as for long-term perspectives for air pollution control. In this study, within the framework of CareBeijing-2006, two sites were established in urban and suburban regions of Beijing between 14 August and 10 September 2006. Trace gas concentrations and meteorological parameters were obtained at both sites, which provided a good opportunity for studying the O_3 chemistry in the polluted Beijing area. The major purpose of the present study is to estimate the gross photochemical ozone production rate and its controlling factors for the Beijing area through an integrated analysis based on observation-based approaches.

2. Experiment

2.1. Study Sites

[6] From the middle of August to early September 2006, two sites, PKU and YUFA, were established as part of CareBeijing-2006. The PKU site is located in the urban area of northern Beijing (39.99°N, 116.30°E), and the YUFA site is in the suburban area of southern Beijing (39.51°N, 116.30°E). The distance between the two sites is about 50 km. In summer, the weather of Beijing is dominated by the Asian monsoon and the valley wind, which is mainly southerly during the daytime. In terms of topography, Beijing is bounded by a mountain region to the north and west, while to the south lies the North China Plain. Bohai Bay is approximately 150 km to the east. The major sources of primary air pollutants are located in the southern part of Beijing and the surrounding provinces. The two sites were selected to be in the direction (north–south) of the dominant wind to characterize the influence of the southerly inflow air masses.

2.2. Measurements

[7] At the two sites PKU and YUFA, O_3, NO/NOy, NO/NO_2, SO_2, and CO were measured by TECO models 49C, 42CY, 42CTL (detection limit for NO: 50 parts per trillion (ppt)), 43C, and 48C, respectively. Daily calibration was carried out routinely. At the same time, 45 species of nonmethane hydrocarbons (NMHCs), C_2–C_{12}, were measured and identified by gas chromatography–flame ionization detector (GC-FID) or photoionization detector (PID) techniques at YUFA, and 50 species of NMHCs (C_3–C_{12}) were measured and identified by GC-FID at PKU. Details on the construction and validation of these two automated GC systems are described by *Xie et al.* [2008] and *Wang et al.* [2008].

[8] HONO was measured by a wet denuder ion chromatography (WD/IC) [*Su et al.*, 2008b] with a detection limit of 100 ppt and by a long-path liquid absorption photometer (LOPAP) [*Kleffmann et al.*, 2002] with a detection limit of 7 ppt in parallel at both sites. At YUFA, the measured HONO concentrations showed good agreement between the LOPAP and WD/IC systems (r^2 = 0.84, $HONO_{LOPAP}$ = 0.85 × $HONO_{WD/IC}$). However, we chose the LOPAP-measured HONO as the model constraint because of its high precision. At PKU, a combined LOPAP- and WD/IC-measured HONO data set was used because of the relatively large gaps in the LOPAP-measured HONO time series. For the combination, we first performed a linear regression between the observed LOPAP and WD/IC (r^2 = 0.65, $HONO_{LOPAP}$ = 0.32 × $HONO_{WD/IC}$). The WD/IC-measured HONO concentrations were scaled accordingly to fill the gaps in the LOPAP data set.

[9] Measurements of oxygenated VOCs (OVOCs) and H_2O_2 were made only at certain time periods. Ambient OVOCs, including several aldehydes (HCHO and C_2–C_5 aldehydes), methyl vinyl ketone, and methacrolein, were sampled by dinitrophenylhydrazine (DNPH)-coated C_{18} cartridges (Waters and Associates) during 24–29 August and 7 and 8 September at the PKU site and 2–11 September at the YUFA site. Two to four DNPH samples were available from each day. The peroxides (H_2O_2 and methyl hydroperoxide) were measured by high-performance liquid chromatography [*Hua et al.*, 2008] during 11–31 August for the PKU site and 1–12 September for the YUFA site. Combining these results with the WD/IC-measured gas-phase HNO_3 concentrations (detection limit of 50 ppt)

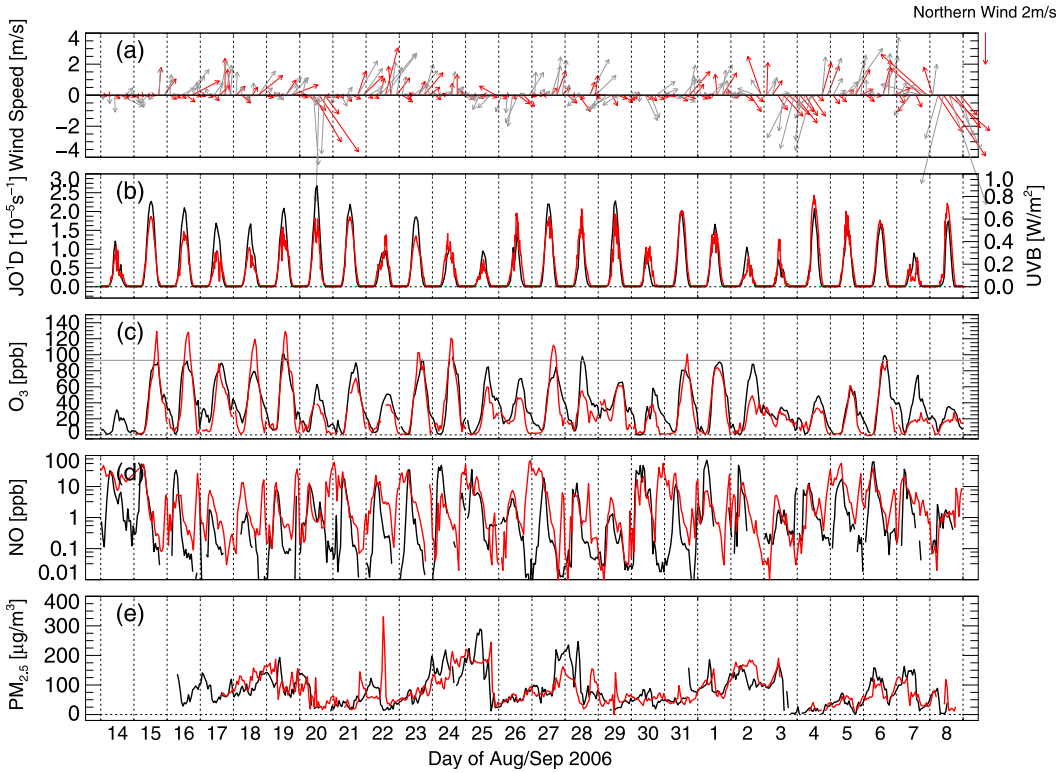

Figure 1. Time series of hourly average data for (a) wind speed, (b) O_3 photolysis frequency ($j(O^1D)$) at the YUFA site in Beijing and UVB at the PKU site in Beijing, (c) O_3, (d) NO, and (e) particulate matter $PM_{2.5}$ at the PKU (red) and YUFA (black) sites. The horizontal line in Figure 1c denotes the hourly averaged national air quality standard for O_3 of 200 μg m^{-3} (about 93 ppbv at 25°C and 1 atm). Vertical dotted lines indicate the zero hour of each day.

makes it possible for us to examine the ratio H_2O_2/HNO_3 as an indicator of O_3 formation.

[10] At the YUFA site, HO_x radicals, total OH reactivity, and photolysis frequencies were also measured. The HO_x concentration was measured by the laser-induced fluorescence (LIF) technique. The 2σ uncertainties from calibration were about 20% [*Holland et al.*, 2003], and the precision of OH and HO_2 at integration times of 5 min was about (0.5×10^6 cm^{-3} + 0.06[OH]) and (0.2×10^8 cm^{-3} + 0.09[HO_2]), respectively. The total atmospheric OH reactivity, k_{OH}, is defined as the pseudo first-order rate coefficient of the sum of all atmospheric OH loss reactions:

$$k_{OH} = \sum k_{OH+X_i}[X_i], \quad (1)$$

where X_i represents the species such as CO, CH_4, O_3, NO_2, HCHO, and VOC. In this study, k_{OH} was directly measured by a UV pump and LIF probe technique similar to that of *Sadanaga et al.* [2004]. In the measurement range of 1–100 s^{-1}, the accuracy of k_{OH} was 7% of the measured value plus 0.3 s^{-1}, and the 1σ precision was 4%–10% (S. R. Lou, personal communication, 2008). The photolysis frequencies were measured by a spectroradiometer [*Bohn et al.*, 2008]. Radiometers were calibrated against the reference spectroradiometer at Forschungzentrum Jülich before and after the study.

[11] Surface meteorological parameters were obtained by a Vaisala Weather Transmitter WXT520 and R.M. Young meteorological station for the PKU and YUFA sites, respectively. The particulate matter $PM_{2.5}$ was measured by a TEOM 1400a at both sites as well.

2.3. Observation-Based Model

[12] In this study, an observation-based model developed by *Cardelino and Chameides* [1995] was used to investigate $P(O_3)$-NO_x-VOC sensitivity through the relative incremental reactivity (RIR). The OBM is a 0-D box model performed with a carbon bond mechanism 4 (CBM4) reaction scheme [*Gery et al.*, 1989; *Dodge*, 2000]. Measurements of O_3, HONO, NO, CO, NMHCs, photolysis frequencies, H_2O, temperature, and pressure were used as model constraints with 1 h intervals. Initial values of the constrained long-lived species were also taken from the measurements. Initial values of the unconstrained trace gas species were set to zero. Calculations of OH, HO_2, RO_2, Peroxyacyl nitrate (PAN), NO_2, and oxidized VOCs were made in a time-dependent mode including their entrainment losses parameterized by the Ozone Isopleth Plotting with Optional Mechanisms version 4 model [*Hogo and Gery*, 1988]. To parameterize entrainment losses, the maximum and minimum heights of the mixing boundary layer were required. Based on lidar measurements at the Sino-Japan Friendship Centre for Environmental Protection (116.3°E, 39.9°N), general maximum and minimum mixing boundary heights in Beijing during the field study were estimated to be 1.5 and

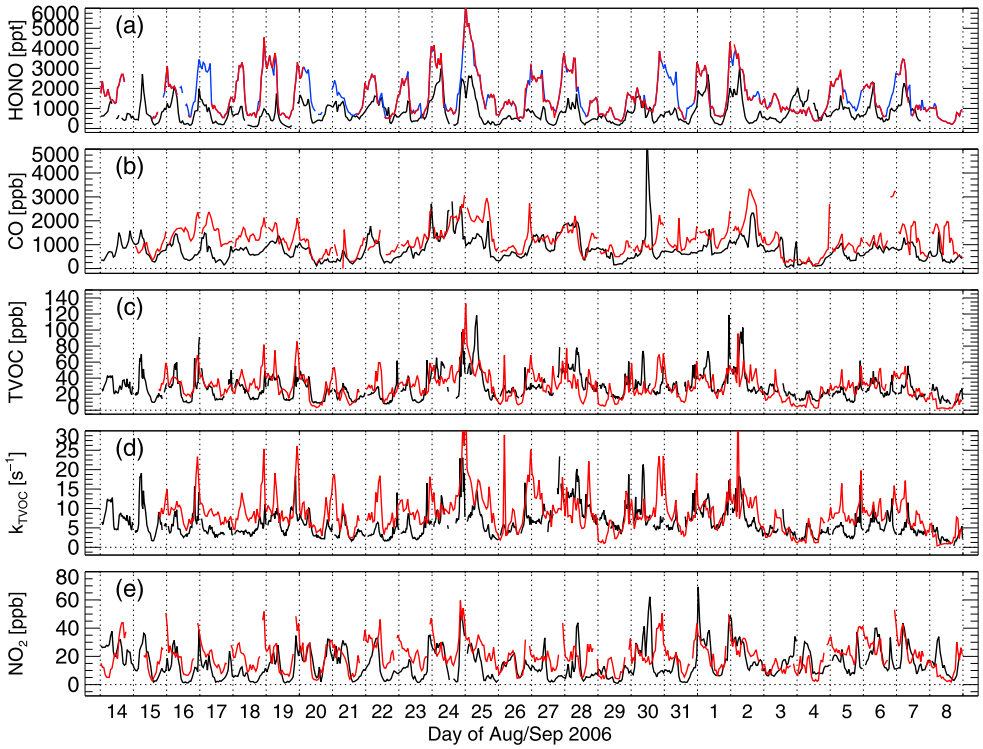

Figure 2. Time series of hourly average data for (a) HONO, (b) CO, (c) TVOC, (d) k_{TVOC}, and (e) NO_2 at the PKU (red and blue) and YUFA (black) sites in Beijing. Red and blue lines in Figure 2a represent the observed HONO concentration at the PKU site by long-path liquid absorption photometry and wet denuder ion chromatography, respectively. Vertical dotted lines indicate the zero hour of each day.

0.5 km, respectively (X. G. Liu, personal communication, 2008). Free tropospheric concentrations of all species were assumed to be zero. The OBM is designed to perform two-phase simulations. The first phase of simulation assimilates the concentrations of specified species to calculate unspecified species and pseudo-emission terms, $S(X)$, for the measured long-lived species. In the second phase, the calculated pseudo-emission terms are varied to test the model sensitivity of precursors. Then the RIR can be determined for NO, CO, NMHCs, and other species as follows:

$$RIR_X = \frac{[P_{O_3-NO}(X) - P_{O_3-NO}(X - \Delta X)]/P_{O_3-NO}(X)}{\Delta S(X)/S(X)}. \quad (2)$$

Here, P_{O_3-NO} is the daytime integrated $P(O_3)$ weighted by the mixed layer height, and it is used as a measure of ozone formation potential [*Carter and Atkinson*, 1987]. If P_{O_3-NO} is replaced by the instantaneous $P(O_3)$, the derived RIR is then denoted as RIR*. RIR* is useful in searching for instantaneous ozone sensitivity.

3. Time Series of Major Parameters

[13] A summary of time series of hourly averaged O_3 photolysis frequency ($j(O^1D)$), UVB, O_3, NO, $PM_{2.5}$, HONO, CO, the total measured VOC concentration (TVOC), the total measured VOC reactivity (k_{TVOC}), and NO_2 at the YUFA and PKU sites is depicted in Figures 1 and 2. The 4 h average wind speeds at both sites are shown in Figure 1a. The GC-measured alkanes, alkenes, and aromatics were summed up as TVOC. The TVOC reactivity is a measure of TVOC based on OH reactivity:

$$k_{TVOC} = \sum k_i[VOC_i], \quad (3)$$

where k_i is the reaction rate constant for the reaction

$$OH + VOC_i \rightarrow \text{peroxyradicals}. \quad (4)$$

The k_i were taken from the work of *Atkinson et al.* [2001] (http://www.iupac-kinetic.ch.cam.ac.uk) and *Chang et al.* [2005].

[14] Among the parameters listed above, $PM_{2.5}$ is a valuable air quality-meteorological index, which tends to vary periodically with large dynamics. The low-$PM_{2.5}$ events of 20, 21, 25, 26, and 28–31 August and 3–5 September corresponded mostly to northerly wind conditions, whereas the other pollution episodes corresponded to southerly wind and/or stagnant conditions. As mentioned above, in general, northerly winds with high wind speeds bring cleaner air from the mountain region, while southerly winds bring emissions over southern Beijing and the surrounding area. Therefore, variations in $PM_{2.5}$ concentration can generally demonstrate the basic pattern of how atmospheric dynamics influences air pollution status. Furthermore, O_3 concentrations at the two sites varied similarly at comparable concentration levels over the entire set of observations. This was also the case for the observed concentrations of $PM_{2.5}$. The similarities of these

two major air pollutants reflected the regional-scale characteristics of air pollution over urban and suburban areas of Beijing.

[15] Compared to the Chinese national air quality standard (approximately 93 ppbv of hourly averaged O_3 concentration at 25°C and 1 atm; horizontal line in Figure 1c), the frequency of O_3 exceedance at both sites could be up to 50%. This is lower than previously reported values for the Beijing area [*Wang et al.*, 2006] and that observed in the Pearl River Delta region in southern China [*Zhang et al.*, 2008b]. Days with relatively low O_3 concentrations, such as 14, 20, 22, 25, 26, 29, and 30 August and 3–5 and 8 September, corresponded to conditions with high wind speeds (especially northerly winds) or low radiation (indicated by $j(O^1D)$ and UV) at the two sites.

[16] At both sites, afternoon NO concentrations were typically either around or less than several hundred parts per trillion by volume (Figure 1d). This was quite surprising since these two sites were both not far from vehicle sources (about 50 m from the nearest roads). The NO concentration at the PKU site was in general higher than that at the YUFA site. This was reasonable because the traffic around PKU was denser than that around YUFA. Daytime NO_2 concentrations at both sites, but especially at the YUFA site, were relatively low for most days and mostly below 5 ppbv during afternoon hours (Figure 2e). Low values of NO_2 were consistent with the observations of low NO concentrations at both sites.

[17] Relatively high HONO concentrations were measured at the YUFA and PKU sites (Figure 2a). Typical daytime HONO concentrations were about several hundred parts per trillion by volume for the YUFA site and 1 ppbv for the PKU site. Compared with the recently reported high HONO observations at a German forest site [*Kleffmann et al.*, 2005], New York [*Ren et al.*, 2003], Berlin [*Alicke et al.*, 2003], and Guangzhou [*Su et al.*, 2008a, 2008b], the observations reported here were among the highest levels. *Richter et al.* [2005] analyzed the spatial distribution of NO_2 according to satellite observations by the Global Ozone Monitoring Experiment and the Scanning Imaging Absorption Spectrometer for Atmospheric Cartography on Envisat. Their results clearly demonstrated the existence of a large high-NO_2 region (about 10° in latitude and 12° in longitude) including Beijing and its surrounding areas. Thus the high HONO concentration observed here and its possible impact on the photochemical ozone production examined in this study may have regional implications. A detailed closure study on HONO chemistry will be presented in a future publication. In the present study, since accurate measurements of HONO concentrations were achieved with LOPAP, they were used as the model constraint to reduce the uncertainty of the unknown sources of HONO in the current photochemical mechanism, which would help in simulating the photochemical $P(O_3)$ and determining how it is formed.

[18] High CO concentrations were also observed at both sites (Figure 2b). The peak value was about several ppmv, while the low value approached 100–200 ppbv at high wind speeds (especially with northerly winds). The TVOCs were comparable at the two sites (Figure 2c), and around noon, they varied between 10 and 30 ppbv. According to *Xie et al.* [2008], on average the major contributors to TVOC were alkanes (57%), aromatics (32%), alkenes (9%), and isoprene (2%) at the PKU site. For the YUFA site, the contributions to TVOC from these different VOC groups were 53%, 21%, 24%, and 2%, respectively.

[19] The k_{TVOC} around noon typically varied between about 4 and 10 s^{-1} at the PKU site and between 2 and 6 s^{-1} at the YUFA site (Figure 2d). Isoprene significantly contributed to k_{TVOC} in the afternoon. The contribution of isoprene between 1100 and 1500 LT was on average about 36% at both sites. However, the online GC-measured VOC reactivity was typically two to three times smaller than the directly measured k_{OH}. Therefore, the role of isoprene was also comparably smaller. Concentration of HCHO and total concentration of C_2–C_5 aldehydes (ALD2) were among the few off-line DNPH measurements. The mean concentration of HCHO was estimated to be 9.2 and 6.1 ppb at the PKU and YUFA sites, respectively, and the mean concentration of ALD2 was estimated to be 7.7 and 5.6 ppb for the PKU and YUFA sites, respectively. Taking these two species into account, another 5 and 3.6 s^{-1} would be contributed to the measured k_{TVOC} for the PKU and YUFA sites, respectively. This could further reduce the difference between the measured k_{TVOC} and the directly measured k_{OH}.

[20] Moreover, the mean OH reaction rate constant, $k_{OH+TVOC}$, can be defined as

$$k_{OH+TVOC} = k_{TVOC}/[TVOC]. \quad (5)$$

During the daytime, $k_{OH+TVOC}$ at the PKU site was higher than 10×10^{-12} cm^3 s^{-1}, which was higher than the OH reaction rate constant of ethene, while the $k_{OH+TVOC}$ values at the YUFA site were mainly from 3×10^{-12} to 10×10^{-12} cm^3 s^{-1}. The difference in $k_{OH+TVOC}$ at these two sites suggested that the PKU site was probably closer to the source and experienced more fresh emissions. *Shao et al.* [2005] estimated $k_{OH+TVOC}$ from the samples obtained within the Beijing area in 2002. Their results were comparable to ours at the PKU site. The mean OH reaction rate constant in the Beijing area was generally higher than that observed in the United States, and it can be considered to be an indication of the intense photochemistry in China [*Shao et al.*, 2005, and references therein].

[21] On all accounts, NO_x, k_{TVOC}, $k_{OH+TVOC}$, CO, HONO, and HCHO were generally higher at the PKU site than at the YUFA site. This gives us a clear means of distinguishing the urban and suburban areas in Beijing.

4. Estimation of Photochemical O_3 Production Rate

[22] Before investigating the $P(O_3)$-NO_x-VOC sensitivity for a certain location, it is useful to estimate the instantaneous $P(O_3)$, which can be used to judge to what extent the present O_3 was formed through local photochemical reactions. If the local formation dominates, we can then focus on the cases of large local photochemical production. The concept of "total oxidant" ($O_x = O_3 + NO_2$) has been frequently used to infer photochemical O_3 production on local, regional, and global scales since it was proposed by *Liu* [1977] and *Levy et al* [1985]. A major advantage of this definition is that its production and loss are independent of the rapid photochemical reactions that convert O_3 to NO_2

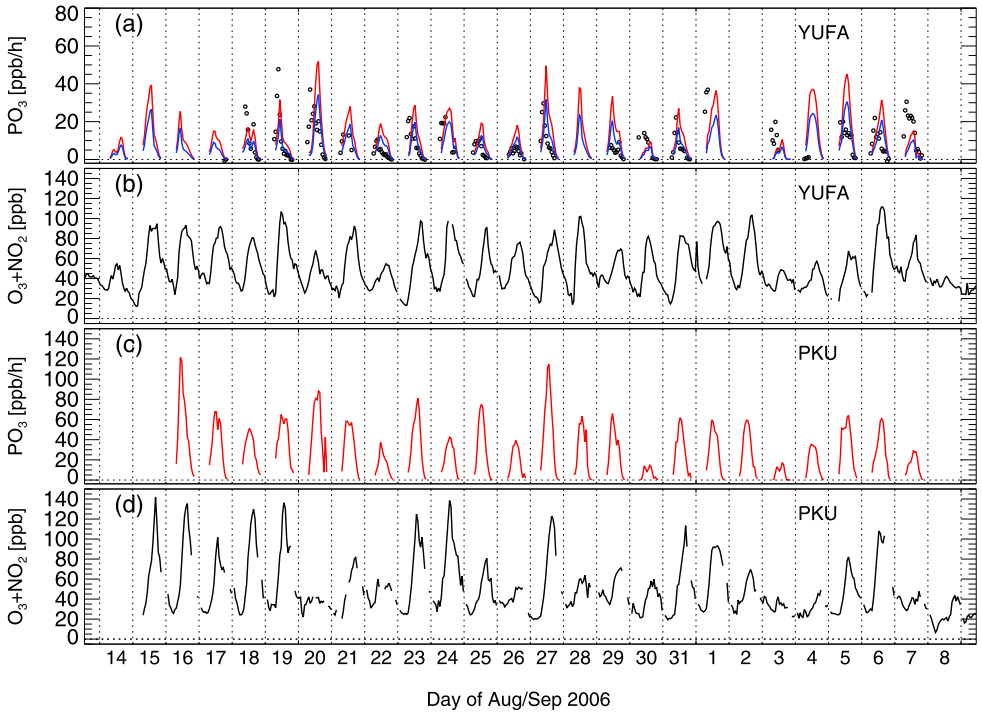

Figure 3. Time series of hourly average data for the observation-based photochemical box model (OBM)-calculated (a, c) $P(O_3)$ (red) and (b, d) $O_3 + NO_2$ at the YUFA and PKU sites, respectively. The $P(O_3)$ proxies $k[HO_2(obs)][NO]$ and $k[HO_2(mod)][NO]$ are given as circles and blue lines in Figure 3a, respectively. Vertical dotted lines indicate the zero hour of each day.

and vice versa. Since these reactions are very fast in the urban and suburban atmosphere, bypassing them enables O_x production to represent the real photochemical production of O_3. In another sense, O_x concentration is a better measure of the real production of oxidant than O_3. With the total oxidant concept, the most useful way to calculate $P(O_3)$ is through

$$P(O_3) = k_{HO_2+NO}[HO_2][NO] + \sum k_{RO_2+NO}\,\phi[RO_2][NO]. \quad (6)$$

[23] Here, ϕ is the yield of NO_2 from the RO_2 + NO reaction. However, it is still very difficult to directly measure peroxy radicals due to their low atmospheric concentration and short lifetime. Only chemical ionization mass spectrometry and matrix isolation electron spin resonance techniques have been able to measure both HO_2 and RO_2 concentrations accurately [*Edwards et al.*, 2003; *Mihelcic et al.*, 2003]; in a relatively clean environment, the peroxy radical chemical amplification technique also functions well [*Volz-Thomas et al.*, 2003]. Otherwise, the LIF technique can be used to measure only HO_2 concentrations [*Heard and Pilling*, 2003]. Therefore, in previous studies, a number of observation-based approaches were formulated to estimate peroxy radical concentrations through photochemical box models, NO_x photostationary states, HO_x radical budgets, and others [*Kleinman*, 2000, and references therein]. In the following, the term "$P(O_3)$" is used throughout to refer to the sum in equation (6) with the OBM-diagnosed peroxy radical and the measured NO. For each RO_2 + NO reaction channel, the corresponding parameter ϕ is the stoichiometric coefficient of the produced NO_2 in the CBM4 mechanism. In addition, calculations of two other $P(O_3)$ proxies using equation (6) with measured or modeled HO_2 and measured NO that omit the RO_2 term are denoted $k[HO_2(obs)][NO]$ or $k[HO_2(mod)][NO]$ in the following discussion.

[24] Temporal variations of $P(O_3)$ calculated by the OBM for the YUFA site are presented as red lines in Figure 3a. For reference, the measured $O_3 + NO_2$ is shown in Figure 3b, and the two $P(O_3)$ proxies $k[HO_2(obs)][NO]$ and $k[HO_2(mod)][NO]$ at the YUFA site are shown as circles and blue lines, respectively, in Figure 3a. At YUFA, the daily maximum $P(O_3)$ values varied from 10 to 50 ppbv h^{-1} and those of $k[HO_2(mod)][NO]$ varied between 5 and 30 ppbv h^{-1}. The daily maximum of $k[HO_2(obs)][NO]$ varied within the range 10–30 ppbv h^{-1} from day to day. It can be seen that the scales of $k[HO_2(obs)][NO]$ and $k[HO_2(mod)][NO]$ are similar. This agreement supports the high $P(O_3)$ values calculated by the OBM model. The O_x concentrations at YUFA showed relatively regular diurnal variations, with an average daytime accumulation of 45 ppbv (Figure 3b). This increase is consistent with the calculated photochemical formation.

[25] The corresponding data for the PKU site are given in Figures 3c and 3d. On average, the photochemical formation rate at PKU was much larger than that at YUFA, and the daily maximum values of $P(O_3)$ varied between 15 and 120 ppbv h^{-1}, while the average daily O_x accumulation was about 47 ppbv. The $P(O_3)$ or its proxies at the two sites were comparable to previously reported values at other urban locations. For example, in Mexico City, maximum values of $k[HO_2(obs)][NO]$ and $k[HO_2(mod)][NO]$ were up to 46 and

86 ppbv h^{-1}, respectively [*Shirley et al.*, 2006]. In Houston, high $P(O_3)$ values (~100 ppbv h^{-1}) were calculated and confirmed by aircraft measurements of O_3 [*Ryerson et al.*, 2003; *Daum et al.*, 2004]. In Tokyo, New York, and Nashville, over the mean or median diurnal profiles, high values of $k[HO_2(obs)][NO]$ or $k[HO_2(mod)][NO]$ were in the range of 10–20 ppbv h^{-1} [*Martinez et al.*, 2003; *Ren et al.*, 2003; *Kanaya et al.*, 2008]. The smallest value of $k[HO_2(obs)][NO]$ for urban locations was observed during the Berliner Ozonexperiment (BERLIOZ), where only about 3 ppbv h^{-1} was demonstrated [*Holland et al.*, 2003].

[26] Nevertheless, for the Beijing area, especially for the urban PKU site, the model-diagnosed O_3 formation was much larger than the observed accumulations. This discrepancy could not be balanced by the major known chemical losses of O_x, for example, the reaction of OH with NO_2 and O_3 photolysis. We calculated the reaction rate of these two O_x losses based on the measured and/or modeled OH and measured NO_2, O_3, and $j(O^1D)$. The sum of these two chemical losses of O_x would be about several parts per billion by volume per hour, which would only slightly change the calculated $P(O_3)$. Hence, losses of O_x through physical processes including vertical and horizontal transport and dry deposition should have contributed significantly.

[27] According to the measured meteorological and photochemical parameters shown in Figures 1 and 2, three kinds of meteorological conditions were distinguished. The first condition was the "southerly wind" days (15–19, 21, 23, 24, and 27 August and 1, 2, 5, and 6 September). As seen in Figure 1, the southerly wind days generally occurred with high peaks in O_3 concentration. The second condition was the "northerly wind" days (20, 25, 26, and 28–31 August and 4 September), and the last condition was the "low-radiation" days (22 and 30 August and 3 and 7 September). This classification is useful because the different source regions for the Beijing areas were affected by the different wind directions as described above. Similar to the analysis applied in Tokyo [*Kanaya et al.*, 2008], the hourly average diurnal profiles of $P(O_3)$, O_x, $2k_{TVOC} \times OH$, $\Delta(O_3 + NO_2)$, and $\Delta(O_3 - NO)$ are presented in Figure 4 under these three conditions for the YUFA and PKU sites. According to the O_x profiles for both sites, larger $P(O_3)$ was expected on southerly wind days than on northerly wind and low-radiation days. However, the values of $P(O_3)$ for southerly and northerly wind conditions were similar at the YUFA site, and this behavior was supported by the variations of $k[HO_2(obs)][NO]$. Hence, the occurrence of smog in the Beijing area appears to be strongly determined by meteorological factors in combination with photochemistry. Under the southerly wind conditions and due to the blocking effect of the northern mountains, pollutants and photochemically produced O_3 accumulated and high O_3 episodes occurred in the northern Beijing urban area where the PKU site was located. However, under the northerly wind conditions, the relatively clean air mass from the mountain region and the O_3 produced could be further diffused to the large southern plain region. This would probably form a more homogeneous distribution of O_3 regionally.

[28] The terms $2k_{TVOC} \times OH$, $\Delta(O_3 + NO_2)$, and $\Delta(O_3 - NO)$ are considered additional $P(O_3)$ proxies that do not rely on the model mechanism in this context. The term $2k_{TVOC} \times OH$ parameterizes the oxidation rate of ambient VOC with a mechanistic reactivity parameter φ_i (in the form $\sum k_i[VOC_i] \times [OH]\varphi_i$) to relate it to the photochemical ozone production, where φ_i describes the chemical yield of O_3 after one molecule of removal of VOCs. As argued by *Kleinman et al.* [2002], φ_i could be parameterized as 2 for polluted areas. The mean diurnal profile of the measured OH concentrations at the YUFA site was used for these calculations at both sites. This term includes the O_3 production potential from all the measured VOCs. In our case, this flux was smaller by a factor of 2–5 than the model-calculated $P(O_3)$ at both sites. The other two terms, $\Delta(O_3 + NO_2)$ and $\Delta(O_3 - NO)$, calculate the neighbor difference over the 1 h averaged $O_3 + NO_2$ or $O_3 - NO$ concentration time series for each site, which in principle would give similar results to $P(O_3)$ when only chemical processes were considered. As shown in Figures 4g–4j, both of them diagnosed similar values, which, however, are much smaller than the model-calculated $P(O_3)$. This difference may indicate that the meteorological factors played a significant role in determining the local near-surface ozone concentrations.

[29] To further evaluate the model calculations, the k_{TVOC}/NO dependence of $P(O_3)$ and its proxies $k[HO_2(obs)][NO]$, $k[HO_2(mod)][NO]$, and $2k_{TVOC} \times OH$ during daytime (0800–1800 LT) was analyzed as shown in Figure 5. In the k_{TVOC}/NO coordinates, typically large $P(O_3)$ values were present in the low-k_{TVOC}/NO regime. The dependence was similar for $P(O_3)$ and the two other proxies, $k[HO_2(obs)][NO]$ and $k[HO_2(mod)][NO]$, when k_{TVOC}/NO was greater than 1 s^{-1} ppb^{-1}. When k_{TVOC}/NO was less than 1 s^{-1} ppb^{-1}, relatively large deviations were observed between $P(O_3)$ and the other proxies, and the values of $k[HO_2(obs)][NO]$ could be much greater than the $P(O_3)$ under this condition. This deviation may imply that the OBM underestimated the HO_x sources in the low-k_{TVOC}/NO regime, which indicates a potential tendency in predicting VOC-sensitive chemistry. However, the real tendency is difficult to explore in the present study because there were no corresponding measurements of RO_2. According to the results from previous field measurements [*Mihelcic et al.*, 2003; *Volz-Thomas et al.*, 2003], the RO_2/HO_2 ratio was highly variable and could be much larger than 1 in a medium- or low-NO_x regime (equivalent to a medium- or high-k_{TVOC}/NO regime). Therefore, the functional dependence between the k_{TVOC}/NO and the real $P(O_3)$ rates may differ significantly from that solely estimated by $k[HO_2(obs)][NO]$. Unlike the other three calculations, the proxy $2k_{TVOC} \times OH$ demonstrated an almost constant level across the entire range. The values of $k[HO_2(obs)][NO]$ were 2–5 times higher than that estimated with the measured OH multiplied by k_{TVOC} in most of the k_{TVOC}/NO dynamics. This discrepancy may suggest that the online GC only measured less than half of the total VOC reactivity in the atmosphere. In the high-k_{TVOC}/NO region, the $P(O_3)$ proxy $2k_{TVOC} \times OH$ was larger than that derived from the measured HO_2. This reversed discrepancy might be due to the fact that the parameterized factor φ_i in the relation of the oxidation rate to photochemical ozone production was no longer equal to 2 at high k_{TVOC}/NO values.

[30] Figures 5a and 5b show $P(O_3)$ and its proxy $k[HO_2(mod)][NO]$ diagnosed by sensitivity model runs without using measured HONO as an input. On the basis

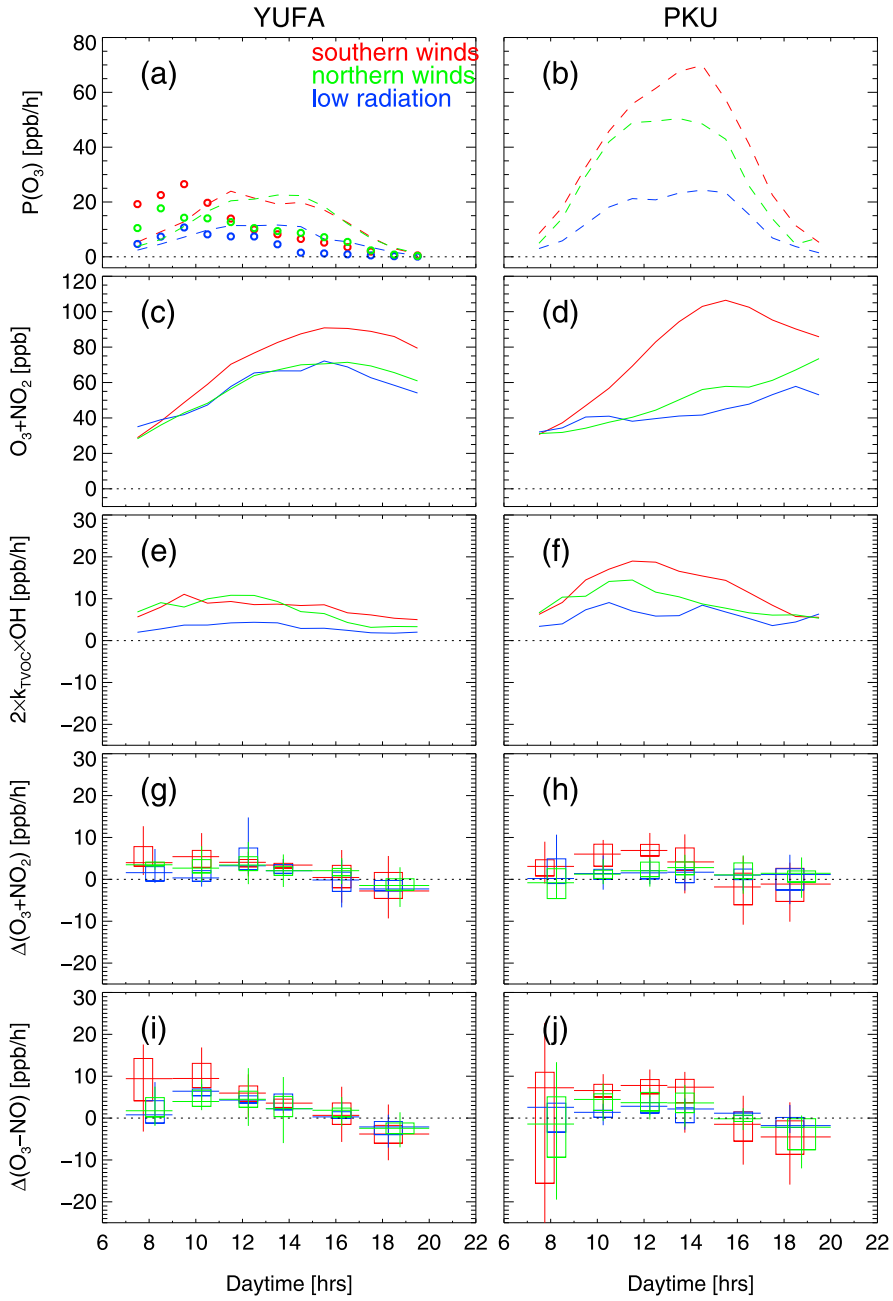

Figure 4. Hourly average diurnal profiles of (a, b) $P(O_3)$, (c, d) O_x, (e, f) $2k_{TVOC} \times OH$, (g, h) $\Delta(O_3 + NO_2)$, and (i, j) $\Delta(O_3 - NO)$ for YUFA and PKU sites, respectively, on southerly wind days (15–19, 21, 23, 24, and 27 August and 1, 2, 5, and 6 September; red), northerly wind days (20, 25, 26, and 28–31 August and 4 September; green), and low-radiation days (22 and 30 August and 3 and 7 September; blue). In Figures 4a and 4b, dashed lines indicate $P(O_3)$ values calculated by the OBM model. In Figure 4a, circles indicate the $P(O_3)$ proxy $k[HO_2(obs)][NO]$. In Figures 4e and 4f, the mean diurnal profile of observed OH concentration at YUFA was used for both sites.

of these comparisons, two important points are found. First, the modeled cases constrained by the measured HONO would lead to a twofold to fourfold increase in the modeled $P(O_3)$ compared to the modeled cases without the measured HONO as an input. These increases were larger for lower k_{TVOC}/NO values. Second, as illustrated in Figure 5b, the modeled cases constrained by the measured HONO matched the measurements better than the modeled cases without the measured HONO as an input. Similar large increases in the modeled $P(O_3)$ could also be found at the PKU site when no direct peroxy radical measurements were available for validation. As interpreted in previous field studies and laboratory investigations [*Alicke et al.*, 2003; *Kleffmann et al.*, 2005; *Kleffmann*, 2007; *Stemmler et al.*, 2006; *Zhang et al.*, 2008b], the difference between the observed and modeled HONO has been considered to be caused

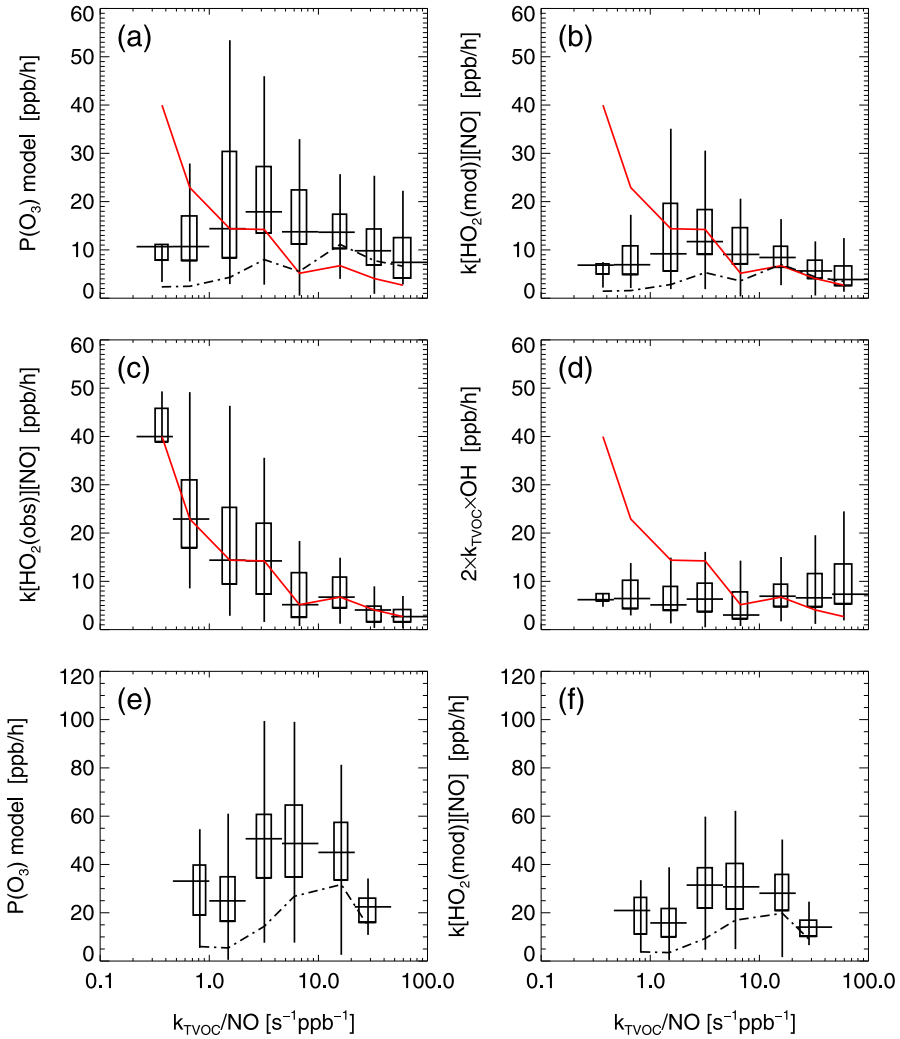

Figure 5. The k_{TVOC}/NO dependence of (a, e) $P(O_3)$ and its proxies (b, f) $k[HO_2(mod)][NO]$, (c) $k[HO_2(obs)][NO]$, and (d) $2k_{TVOC} \times OH$. Figures 5a–5d show results from the YUFA site, and Figures 5e and 5f show results from the PKU site. The box-whisker data are over equally spaced log(k_{TVOC}/NO) intervals. The median values of the $P(O_3)$ proxy $k[HO_2(obs)][NO]$ in each k_{TVOC}/NO bin are shown as red lines in Figures 5a–5d. The dash-dotted lines in Figures 5a, 5b, 5e, and 5f depict the median value of $P(O_3)$ or its proxy $k[HO_2(mod)][NO]$ calculated by sensitivity model runs without measured HONO as a model input.

by unknown heterogeneous mechanisms. Hence, similar to what had been discovered for the PRD region [*Zhang et al.*, 2008b], the results we obtained may indicate the importance of heterogeneous contributions of HONO to photochemical O_3 production in Beijing urban and suburban areas. If these heterogeneous productions of HONO could be attributed to reactions on the aerosol surface and atmospheric NO_2 was involved, our results would suggest the importance of aerosols and NO_2 in the chemistry for the Beijing area and the unique importance of reducing NO_x before considering the regime of O_3 formation. Moreover, the k_{TVOC}/NO dependence of the calculated $P(O_3)$ for modeled cases with or without the measured HONO as an input were different at the two sites. The $P(O_3)$ of the modeled cases without the measured HONO as input demonstrated a peak shifted toward the larger-k_{TVOC}/NO regime compared to the modeled cases with the measured HONO as an input. This behavior implies a systematic tendency to predict VOC-sensitive chemistry for models without the measured HONO as input, namely, without a heterogeneous HONO source mechanism.

[31] In the next section, we investigate the $P(O_3)$-NO_x-VOC sensitivity on two different time scales: hours and days. The discussion of the former focuses on instantaneous $P(O_3)$, and the latter focuses on O_3 production potentials (P_{O_3-NO}).

5. Photochemical Ozone Production ($P(O_3)$) Nitrogen Oxide (NO_x)–Volatile Organic Compound (VOC) Sensitivity

5.1. Day-to-Day Variations in $P(O_3)$-NO_x-VOC Sensitivity

[32] Daily integrated RIR is an important parameter for evaluating a policy that targets reduction in the 8 h O_3

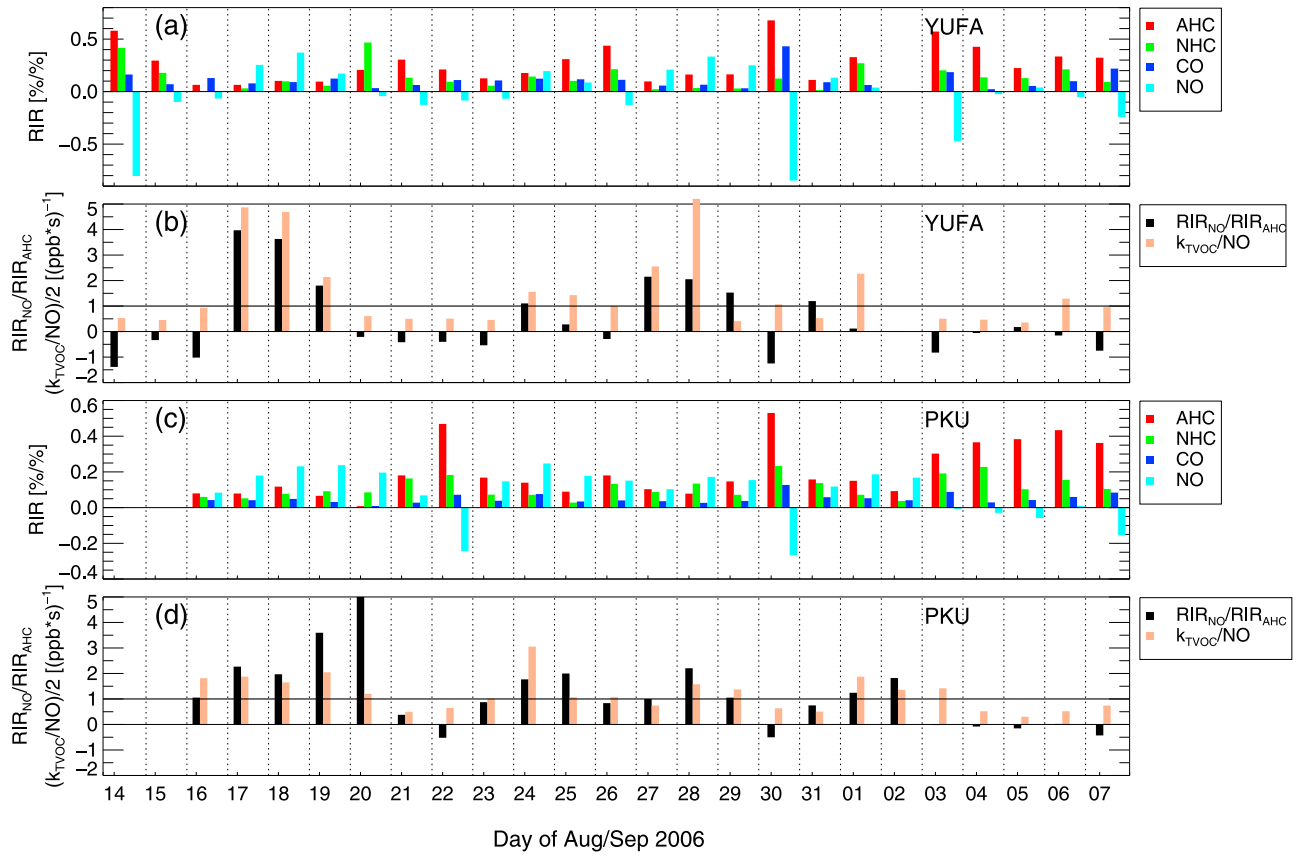

Figure 6. Daily integrated O_3-NO_x-VOC sensitivity judged by OBM-calculated relative incremental reactivity (RIR) values for the YUFA and PKU sites. (a, c) Daily RIR values of anthropogenic hydrocarbons (AHC), natural hydrocarbons (NHC), CO, and NO. (b, d) Daily values of RIR_{NO}/RIR_{AHC} and the daytime average ratio k_{TVOC}/NO.

concentration as required by the ambient air quality standards of many countries. In this study, we calculated daily integrated RIRs for anthropogenic hydrocarbons (AHC, including measured alkanes, alkenes, and aromatics), natural hydrocarbons (NHC, including only isoprene), CO, and NO from 14 August to 7 September (Figure 6). Limited by the availability of measured long-lived species, the RIRs at the YUFA site on 2 September and at the PKU site on 14 and 15 August could not be calculated. The RIR_{NO}/RIR_{AHC} parameter for each day is also presented in Figure 6b as a measure of NO_x-VOC sensitivity. Overall, RIR and NO_x-VOC sensitivity showed large day-to-day and site-to-site variations. At the YUFA site, the NO_x-sensitive days were 17–19, 24, 27–29, and 31 August, and the VOC-sensitive days were 14–16, 20–23, 25, 26, and 30 August and 1–7 September. At the PKU site, the NO_x-sensitive days were 16–20, 24, 25, 28, and 29 August and 1 and 2 September, and the VOC-sensitive days were 21–23, 26, 27, 30, and 31 August and 3–7 September.

[33] Of interest, the NO_x- and VOC-sensitive days did not correspond to the different meteorological conditions, that is, southerly wind, northerly wind, and low-radiation days. In the coordinates of RIR_{NO}/RIR_{AHC} and the daily maximum O_3 concentration, we found that at the YUFA site, the high-O_3 episodes (maximum O_3 within 80–100 ppbv) were partly sensitive to NO_x and to VOC. However, at the PKU site, the high-O_3 episodes (maximum O_3 within 80–140 ppbv) were mostly sensitive to NO_x (Figures 7a and 7b).

[34] Furthermore, RIR_{NO}/RIR_{AHC} was compared to other measured or measurement-derived parameters (daily daytime average NO, TVOC, k_{TVOC}, isoprene, $j(NO_2)$, HONO, temperature, and k_{TVOC}/NO) to identify differences between NO_x- and VOC-sensitive days. None of these parameters demonstrated good correlation with RIR_{NO}/RIR_{AHC} except k_{TVOC}/NO. The daytime average k_{TVOC}/NO ratio is defined as $k_{TVOC}/NO = mean(k_{TVOC})/mean(NO)$. For the YUFA and PKU sites, the correlation coefficients (r^2) between RIR_{NO}/RIR_{AHC} and k_{TVOC}/NO were about 0.6 and 0.5, respectively. The date 20 August was excluded from the correlation analysis since the ratio RIR_{NO}/RIR_{AHC} on this date was strongly distorted by the low value of RIR_{AHC} (Figures 7c and 7d). Daily average k_{TVOC}/NO values for each day are also shown in Figure 6. The variations in RIR_{NO}/RIR_{AHC} basically followed the variations in k_{TVOC}/NO at both sites. Typically, if k_{TVOC}/NO was lower than 2 s^{-1} ppb^{-1}, O_3 production was most likely to be VOC-sensitive chemistry, while if k_{TVOC}/NO was larger than 4 s^{-1} ppb^{-1}, O_3 production was most likely to be NO_x-sensitive chemistry.

[35] However, there were some days (24 and 25 August at the YUFA site and 2 and 3 September at the PKU site) with similar values of k_{TVOC}/NO but for which the OBM predicted significantly different $P(O_3)$-NO_x-VOC sensitivity. In

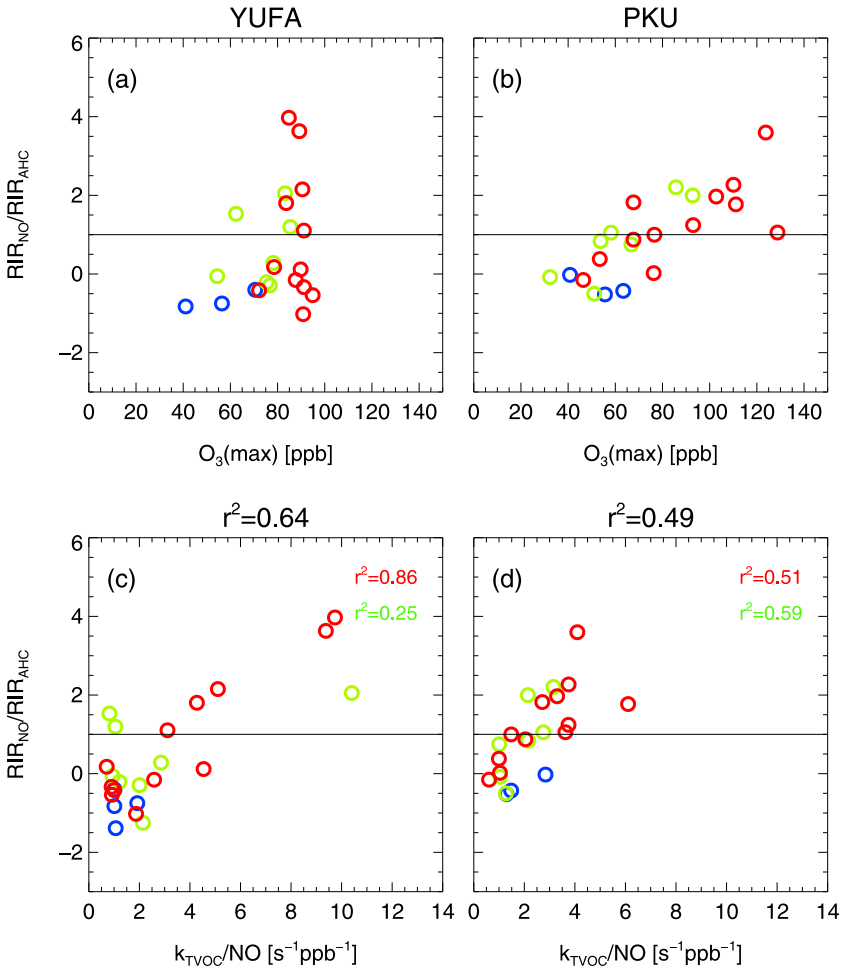

Figure 7. Relationship of RIR_{NO}/RIR_{AHC} to (a, b) daily maximum O_3 concentration and (c, d) ratio of daily average k_{TVOC}/NO at the YUFA and PKU sites, respectively. Data are given for the southerly wind condition (red), northerly wind condition (green), and low-radiation condition (blue). The horizontal line is the division between the NO_x-sensitive and VOC-sensitive regimes.

the following discussions (see section 5.3), the daily integrated RIRs calculated by the OBM would be strongly affected by the time evolution of the weighting factor regarding this prediction, that is, a change in the instantaneous $P(O_3)$ regime or $P(O_3)$ itself. Hence, this kind of variability should be attributed to the different diurnal variation pattern of k_{TVOC}/NO for the different days, which was not reflected by the daytime average ratio k_{TVOC}/NO. Accordingly, we revisited the diurnal variations in k_{TVOC}/NO on 24 and 25 August at the YUFA site. Distinct diurnal patterns of k_{TVOC}/NO were found for those 2 days, and even the daytime average k_{TVOC}/NO ratio was similar. The effective k_{TVOC}/NO ratios corresponding to high $P(O_3)$ were thus also much different. As a result, different O_3-NO_x-VOC sensitivities were predicted for these two days by the OBM. A similar situation was also found on 2 and 3 September at the PKU site. It is worth noting that the changes in the diurnal variations of k_{TVOC}/NO in these two pairs of neighboring days at the two sampling sites corresponded to a distinct change in wind direction. This might imply that a better correlation between RIR_{NO}/RIR_{AHC} and k_{TVOC}/NO might be reached under similar meteorological conditions. Thus, the correlation coefficients of these two parameters (RIR_{NO}/RIR_{AHC} and k_{TVOC}/NO) were calculated separately for the southerly and northerly wind days. At the YUFA site, surprisingly good correlation (r^2 up to 0.8) was found for the southerly wind days, while the r^2 dropped to ~0.25 over the northerly wind days. The relatively poor correlation for the northerly wind days might be due to the significant change in alkene concentrations within this period (Figure 9a). At the PKU site, the separate calculation of r^2 did not significantly improve the correlations between RIR_{NO}/RIR_{AHC} and k_{TVOC}/NO under the two dominant wind conditions. This may be due to the relatively stable speciation of VOC reactivity therein (Figure 9b).

[36] Moreover, we compared the OBM-calculated RIR_{NO}/RIR_{AHC} with the measurement-derived H_2O_2/HNO_3 ratio averaged for the afternoon (1500–1900 LT). The correlation between RIR_{NO}/RIR_{AHC} and the measurement-derived H_2O_2/HNO_3 ratio is shown in Figure 8. No significant correlation between these two parameters was found (r^2 was less than 0.3). Actually, the OBM calculations were not consistent with the measurement-derived H_2O_2/HNO_3 ratio for determining the O_3 formation regime in many occasions. This was probably due to variations in SO_2 concentration levels. As illustrated by the color coding in Figures 8a and

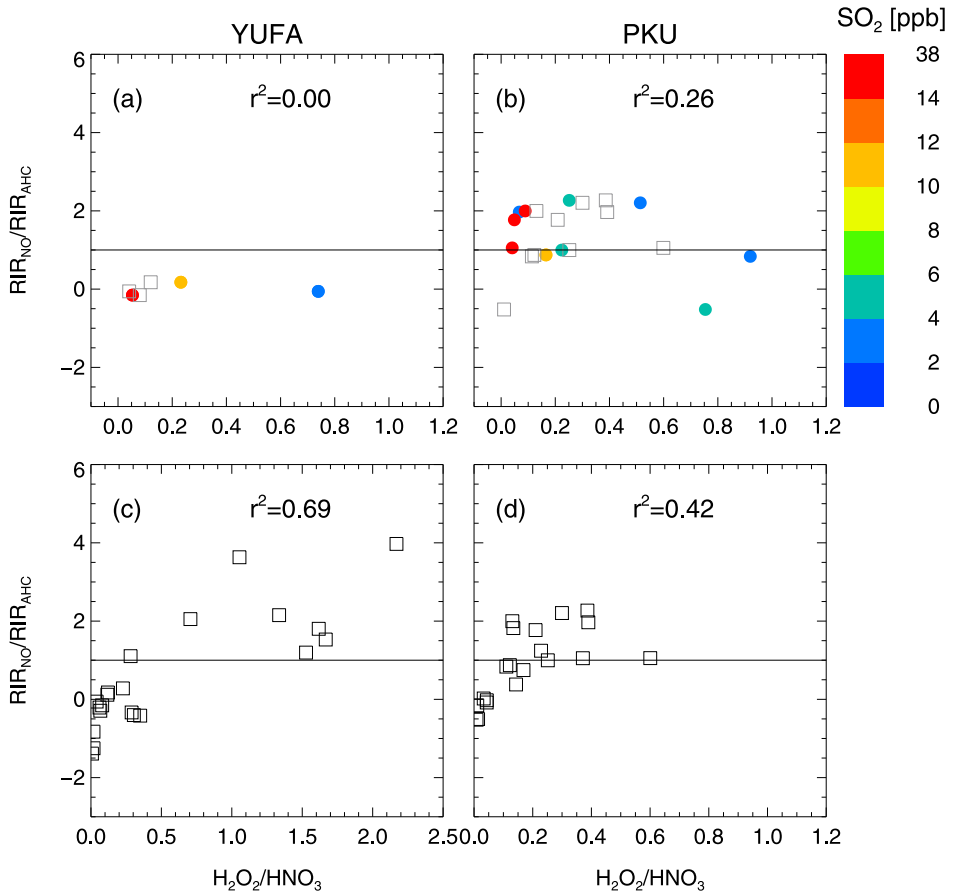

Figure 8. Correlations between RIR_{NO}/RIR_{AHC} and the average H_2O_2/HNO_3 ratio during the afternoon (1500–1900 LT). (a, b) The correlation for measurement-derived values, with the corresponding averaged SO_2 concentration given by colored circles; the corresponding model-derived values are shown as rectangles; the correlation coefficient (r^2) between RIR_{NO}/RIR_{AHC} and the measurement-derived H_2O_2/HNO_3 is also shown. (c, d) The correlation for the model-calculated average H_2O_2/HNO_3 ratio. Limited by the available measurements of H_2O_2 in the afternoon hours, the data coverage is for 4–6 September for the YUFA site and 16–19 and 22–30 August for the PKU site. The horizontal line in each panel marks the division between the NO_x-sensitive and VOC-sensitive regimes.

8b, the H_2O_2/HNO_3 ratios were strongly influenced by SO_2 concentration. This phenomenon indicated that the fast heterogeneous reactions between H_2O_2 and SO_2 could potentially have caused the failure of the H_2O_2/HNO_3 indicator.

[37] Nonetheless, some cases at the PKU site that were located in a similar SO_2 regime had significantly different H_2O_2/HNO_3 ratios. This further suggests that other factors were also important in determining H_2O_2/HNO_3, which might include the processes of HO_x photochemistry, heterogeneous chemistry, and transportation. The effects of heterogeneous chemistry and transportation were probed qualitatively by color coding the above correlations with correspondingly averaged $PM_{2.5}$ concentrations and wind speeds. It was found that the significant variations of H_2O_2/HNO_3 in certain SO_2 regimes seem to be linked to the simultaneous variations of the heterogeneous or transport factors. The effect of HO_x photochemistry is examined semiquantitatively through the correlation between RIR_{NO}/RIR_{AHC} and the modeled H_2O_2/HNO_3 (note that the SO_2 chemistry is not included in CBM4). As shown in Figures 8c and 8d, the modeled relationship displayed a slightly smaller indicator value of H_2O_2/HNO_3 (~0.2–0.3) for the transition regime than did the previous 3-D model calculations (0.4–0.6 [*Sillman*, 1995; *Chen and Chang*, 2006]). The difference is probably due to the use of RIR_{NO}/RIR_{AHC} to determine the O_3-NO_x-VOC sensitivity instead of RIR_{NO}/RIR_{VOC}. On the other hand, in comparing the correlation of the modeled and measured H_2O_2/HNO_3 with RIR_{NO}/RIR_{AHC}, relatively good agreement was found when H_2O_2/HNO_3 was in the range of 0.04–0.4 for the PKU site (Figure 8b). However, low values of H_2O_2/HNO_3 typically mean low H_2O_2 concentrations, which further suggested a relatively large uncertainty in the measurement-derived ratio, and thus the agreement might not be significant.

[38] In the above discussions, we basically understand the day-to-day and site-to-site variations in RIR_{AHC} and RIR_{NO}. However, RIR_{NHC} and RIR_{CO} are still not understood. Moreover, for the VOC-sensitive days, identification of the important VOC groups was needed. Hence, the speciation of the model-calculated daytime average k_{OH} was analyzed. Considering the possible influences of the wind field, the

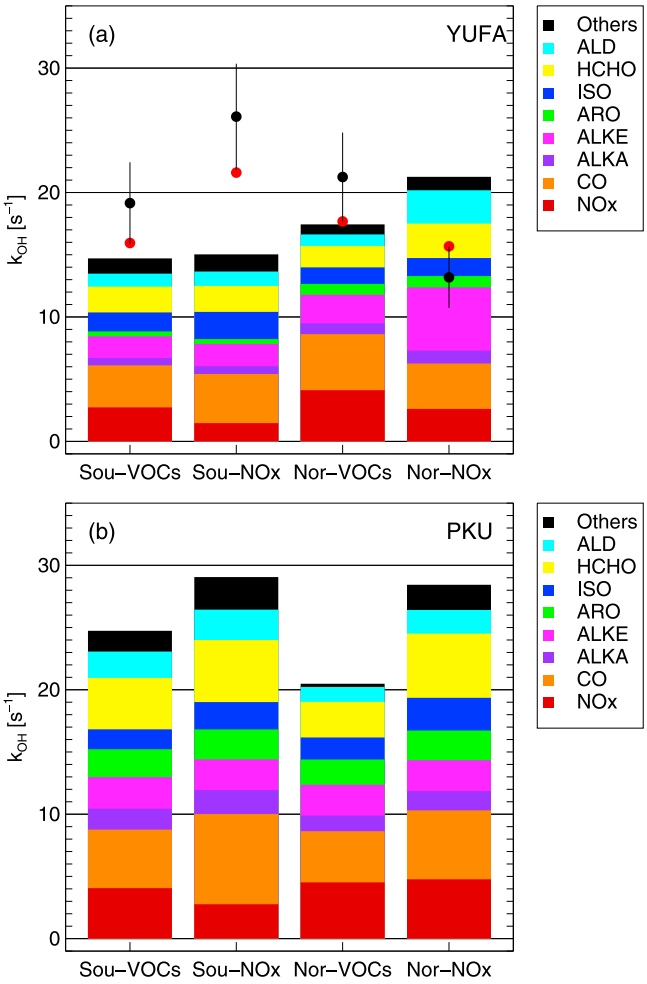

Figure 9. Variation and speciation of daytime average k_{OH} for four cases at (a) YUFA and (b) PKU. The black and red circles in Figure 9a represent the measured and modeled daytime average k_{OH} values, respectively. The error bars of the black circles denote the 2σ uncertainties of the measurement accuracy. ALKA, alkanes; ALKE, alkenes; ARO, aromatics; ISO, isoprene; Nor-NOx, the NO_x-sensitive case for the northerly wind condition; Nor-VOCs, the VOC-sensitive case for the northerly wind condition; Sou-NOx, the NO_x-sensitive case for the southerly wind condition; Sou-VOCs, the VOC-sensitive case for the southerly wind condition.

data set was classified into four cases: southerly wind/VOC-sensitive condition, southerly wind/NO_x-sensitive condition, northerly wind/VOC-sensitive condition, and northerly wind/NO_x-sensitive condition at both the YUFA and PKU sites (Figure 9, vertical bars). The measured and modeled daytime averaged k_{OH} values at the YUFA site are compared in Figure 9a (since the k_{OH} measurements were limited, the mean values of the measured and modeled k_{OH} (circles) are only a subset of the full model results, which show significant differences from what is given at the top of the vertical bars). In each case, the modeled k_{OH} shows agreement with the measured values if the measurement uncertainties are considered. For all four cases, relatively good agreement of the variation trend was also found between the modeled k_{OH} and the measured values. This implied that the present OBM simulated the real atmospheric reactivity relatively well, which was important for the diagnosis of the O_3 production potential.

[39] At both sites, measured NO_x, CO, and NMHCs (alkanes, alkenes, aromatics, and isoprene) in total contributed to more than 60% of the model-diagnosed k_{OH}. The other 40% was mainly due to HCHO and ALD2 calculated by the model. Of interest, the reactivity of the modeled HCHO and ALD2 was comparable to the mean reactivity derived from the DNPH measurements as described above (section 2.2). Thus, the modeled k_{OH} for both sites could also be approximately estimated by measurements of the direct trace gases. Similar to the measured k_{TVOC}, the modeled k_{OH} at the PKU site was higher than that at the YUFA site. This indicated that the urban site (PKU) was influenced by both local emissions and the regional background reflected by the suburban site (YUFA). The OH reactivity from CO was about 3–8 s^{-1} at both sites, contributing approximately 17%–27% of the total k_{OH}. This was consistent with the level of CO concentration and its relatively large RIRs.

[40] At the YUFA site, the VOC reactivity was mainly dominated by isoprene and alkenes. However, under the northerly wind conditions, aromatics contributed significantly. Specifically, under the northerly wind/NO_x-sensitive condition, alkenes had extremely high OH reactivity (about 5 s^{-1}, or 60% of k_{TVOC}). The high aromatic concentration at the YUFA site was probably from urban vehicular emissions in Beijing, while the high alkene concentration was likely from a residual plume from petrochemical industries according to the source apportionment of the VOC species analyzed by a receptor model [*Song et al.*, 2007]. At the PKU site, all four cases showed that the VOC reactivities of alkanes, alkenes, aromatics, and isoprene were comparable. Compared to the YUFA site, substantial increases of aromatics and alkanes were observed, consistent with the large vehicular emissions in urban areas. Besides HCHO, ALD2 also contributed significantly to the total reactivity at both sites. In the box model, contributions of HCHO and ALD2 to O_3 production were accounted for by AHC and NHC through the CBM4 mechanism.

5.2. O_3 Isopleth Diagrams

[41] The relationship between instantaneous $P(O_3)$ and NO_x and k^*_{OH} was investigated by O_3 isopleth-style diagrams (Figure 10) by following the analysis of *Kleinman et al.* [2005]. k^*_{OH} is calculated as the difference between the model-derived k_{OH} and the term k_{OH+NO2} [NO_2], which represents the summed reactivity from measured CO and VOCs and modeled OVOCs. Hence, instead of the extensively discussed parameter k_{TVOC}, k^*_{OH} will be used in this section for better comparison with discussions by *Kleinman et al.* [2005], where the x coordinates include the reactivity of CO, NMHCs, and several estimated OVOCs. In Figure 10, in the photochemical space constituted by NO_x, k^*_{OH}, and $P(O_3)$, the time series of the measured or modeled results are given in a diagram depicting the $P(O_3)$-NO_x-VOC sensitivity graphically. High $P(O_3)$ appears in a region where k^*_{OH}/NO_x is within the range [1, 10] at both sites. Compared with a study of five cities in the United States [*Kleinman et al.*, 2005], the results in Beijing covered a narrower range of VOC reactivity and NO_x. At the YUFA site, NO_x varied by

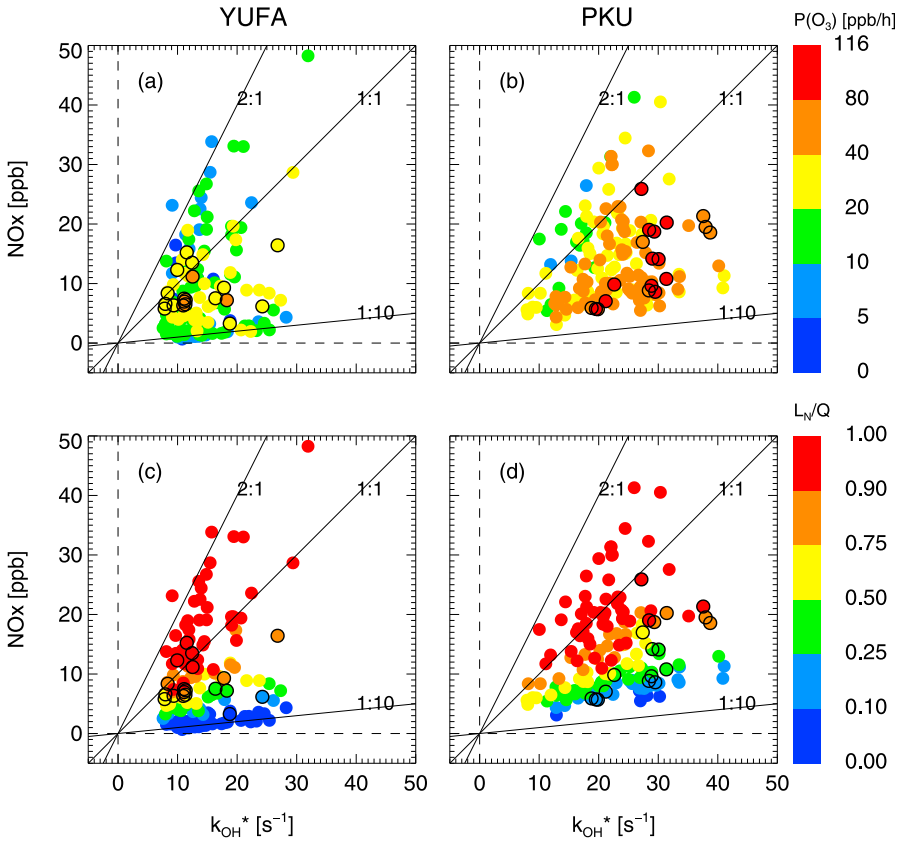

Figure 10. OBM-calculated (top) $P(O_3)$ and (bottom) L_N/Q (fraction of radicals removed by reaction with NO_x related to total radical production rates) for (left) YUFA and (right) PKU as a function of k^*_{OH} (=$k_{OH} - k_{OH+NO_2}$ [NO_2]) and NO_x concentration. Plots are in the style of an O_3 isopleth diagram. Data are ordered from low values of $P(O_3)$ and L_N/Q to high values, so high-$P(O_3)$ (or L_N/Q) samples in some cases are obscuring low-$P(O_3)$ (or L_N/Q) samples. Points with the same values of NO_x and k^*_{OH} can differ by having different values of Q (primary production rate of HO_x radicals). Samples with high $P(O_3)$ values at each site (top 20% of distribution) are indicated by outlined circles. Isolines of constant k^*_{OH}/NO_x are shown.

roughly two orders of magnitude (about 0.5–50 ppbv), while k^*_{OH} showed much less variability (about 6–30 s^{-1}). At the PKU site, the variability in NO_x and k^*_{OH} was small as well (about 2–50 ppbv and 6–40 s^{-1}, respectively). Of interest, as shown in Figure 10b, very high $P(O_3)$ (>80 ppb/h) was found here for Beijing and was reported by *Kleinman et al.* [2005] for Houston, both of which correspond to similar chemical regimes for k^*_{OH} (20–35 s^{-1}) and NO_x (5–20 ppb).

[42] The photochemical space constituted by NO_x, k^*_{OH}, and L_N/Q, where L_N denotes the termination rate of the HO_x radical through reaction with odd nitrogen compounds, and Q represents the sum of the HO_x primary sources, was also investigated (Figures 10c and 10d). The theoretical meaning of using HO_x termination rates or the ratio L_N/Q for judging $P(O_3)$ NO_x-VOC sensitivity has been discussed extensively [*Sillman et al.*, 1990; *Kleinman et al.*, 1997, 2001; *Kleinman*, 2000, 2005; *Sillman and He*, 2002; *Thornton et al.*, 2002]. According to this ratio as calculated by the present OBM model, we found that $P(O_3)$ was primarily sensitive to NO_x when the ratio k^*_{OH}/NO_x was high but was sensitive to VOC when the ratio was low. At the YUFA site, more data points with higher $P(O_3)$ were located in the VOC-sensitive region, while at the PKU site, the opposite occurred. This difference was consistent with the corresponding ratio of k_{OH}*/NO_x, which was also similar to the distribution of the O_3 formation regime for daily maximum O_3 concentrations (Figure 7). As discussed by *Kleinman* [2005], the transition between NO_x- and VOC-sensitive chemistries occurs at $L_N/Q = 1/2$. If L_N/Q is larger than 1/2, the production of O_3 is VOC-limited; otherwise it is NO_x-limited. In our case, the transition regime corresponded to the interface between the green and yellow areas in Figures 10c and 10d. Thus, at both the YUFA and PKU sites, the samples were partially sensitive to NO_x and partially sensitive to VOCs. The high-O_3 subset at these two sites also covered a relatively wide range of L_N/Q values.

5.3. Diurnal Photochemical Development

[43] In a study of U.S. cities, the O_3 production regime was empirically found to transform from a morning VOC-sensitive chemistry to an afternoon NO_x-sensitive chemistry during summer, and the transition regime typically occurred around the time of peak O_3 [*North American Research Strategy for Tropospheric Ozone*, 2000]. In the present study, significant diurnal changes in the O_3 precursors were observed. The averaged diurnal variations in the O_3 production regime characterized by L_N/Q, RIR^*_{NO}, and RIR^*_{AHC} are

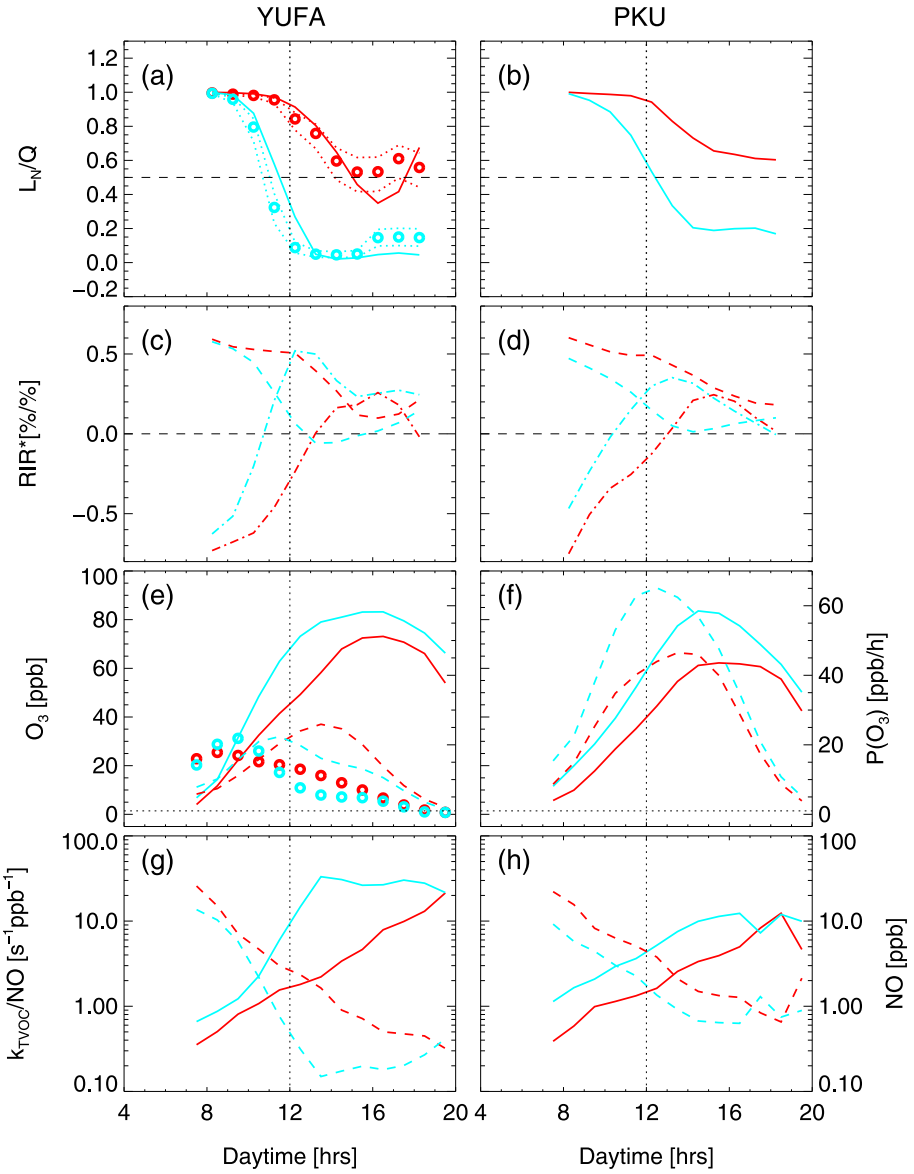

Figure 11. Composite plot of mean diurnal variation in OBM-calculated (a, b) L_N/Q and (c, d) RIR* and (e, f) measured O_3, $P(O_3)$, and (e) $P(O_3)$ proxies $k[HO_2(obs)][NO]$ and (g, h) k_{TVOC}/NO and NO for NO_x-sensitive (cyan) and VOC-sensitive conditions (red) at YUFA and PKU sites classified by the daily integrated RIRs. In Figures 11a and 11b, circles give the measurement-derived L_N/Q values by assuming RO_2/HO_2 equal to 1, dotted lines give the measurement-derived L_N/Q values by assuming RO_2/HO_2 equal to 0.5 or 2, and solid lines give the modeled L_N/Q values. In Figures 11c and 11d, dashed lines give RIR^*_{AHC} and dash-dotted lines give RIR^*_{NO}. In Figures 11e and 11f, circles give $k[HO_2(obs)][NO]$, solid lines give O_3 concentration, and dashed lines give the modeled $P(O_3)$ rates. In Figures 11g and 11h, solid lines give the ratio k_{TVOC}/NO and dashed lines give NO concentration.

presented in Figure 11 for the NO_x-sensitive and VOC-sensitive dates, respectively (classified by the daily integrated RIRs; see Figure 6). Corresponding diurnal variations in O_3 concentration, $P(O_3)$, k_{TVOC}/NO, and NO concentration are also shown for reference.

[44] According to the theoretical calculations for L_N/Q (section 5.2), RIR^*_{NO}, RIR^*_{AHC} (section 2.3), and the transition between NO_x- and VOC-sensitive chemistries can be estimated by $L_N/Q = 1/2$ or $RIR^*_{NO} = RIR^*_{AHC}$. The O_3 production regime judged by the model-calculated L_N/Q exhibited good agreement with the model-calculated RIR^*_{NO} and RIR^*_{AHC} (Figure 11). It was interesting to see that the parameter derived from the HO_x budget worked as well as the parameters derived from a series of sensitivity model runs for the diagnosis of the O_3 production regime. At the YUFA site, based on the assumption of $RO_2/HO_2 = 1$ and an estimate of the rate coefficient of $HO_2 + RO_2$ as twice the rate coefficient of $HO_2 + HO_2$, the termination rates of $HO_x - HO_x$ (including $HO_2 + HO_2$ and $HO_2 + RO_2$) and $HO_x - NO_x$ (including $OH + NO_2$) could be calculated directly from the measured concentrations of OH, HO_2, and NO_2. Since the HO_x budget should be in photochemical equilibrium due to its short life-

time, the parameter Q was set to be equal to the sum of the termination rates of $HO_x - HO_x$ and $HO_x - NO_x$, and the parameter L_N was defined as the termination rate of $HO_x - NO_x$. We could therefore derive the parameter L_N/Q from direct measurement of HO_x radicals. The measurement-derived L_N/Q is shown by circles in Figure 11a. Two additional calculations with RO_2/HO_2 set to 0.5 or 2 were performed to estimate the sensitivity (Figure 11a, dotted lines) because the assumption of $RO_2/HO_2 = 1$ was not a good approximation, especially for the low-NO regime [*Mihelcic et al.*, 2003; *Volz-Thomas et al.*, 2003]. The mean diurnal profiles of measurement-derived L_N/Q values were not very sensitive to the assumed ratio of RO_2/HO_2. Variations by a factor of 2 in the assumed RO_2/HO_2 ratio would only result in less than 10% variation of the calculated L_N/Q. Relatively good agreement between the model- and measurement-derived L_N/Q was reached. From this point of view, the model simulated the diurnal pattern of the O_3 production regime relatively well.

[45] As diagnosed by L_N/Q or RIR^*_{NO} and RIR^*_{AHC}, we found that the transition to NO_x-sensitive conditions occurred around noon at both the YUFA and PKU sites for the NO_x-sensitive days. For the VOC-sensitive days, the NO_x-sensitive conditions appeared in the afternoon, which, however, were transformed into VOC-sensitive conditions shortly afterward at the YUFA site; at the PKU site, the whole day was controlled by the VOC-sensitive chemistry but with a transition trend to the NO_x-sensitive chemistry from morning to afternoon hours. Both sites experienced strong VOC-limited chemistry during early-morning hours. As indicated by the mean diurnal profiles of O_3 concentration, the appearance of the O_3 maximum values did not match the transition regime as expected. However, the time difference in the appearance of the O_3 maximum values between NO_x- and VOC-sensitive days was similar to the time difference in the appearance of the transition regime. Indeed, the O_3 maximum values on NO_x-sensitive days appeared earlier than on VOC-sensitive days. This behavior indicated that the appearance time of the O_3 maximum value might also serve as an indicator of $P(O_3)$-NO_x-VOC sensitivity. In addition, as expected, the maximum values of the modeled $P(O_3)$ occurred prior to the measured maximum of O_3 concentration.

[46] Combining the diurnal profiles of $P(O_3)$ and the O_3 production regime for NO_x-sensitive days, we see that the integrated result show a NO_x-sensitive chemistry as characterized by RIRs (section 5.1) due to more O_3 production occurring in the NO_x-limited regime. The opposite occurred on VOC-limited days. Thus, the uncertainty of the OBM-diagnosed daily integrated RIRs could be attributed to the uncertainty in time variations of $P(O_3)$ and the O_3 production regime. For our case, the time variations of the O_3 production regime were well simulated, while relatively large uncertainties could exist for the diurnal variations of $P(O_3)$. Comparisons of the modeled $P(O_3)$ and its proxies at the YUFA site showed the calculated $P(O_3)$ peak shifting to the larger k_{TVOC}/NO regions relative to the term $k[HO_2(obs)][NO]$ (Figure 5). We found that this shift corresponded to a temporal shift in which the modeled $P(O_3)$ peak appears later than the term $k[HO_2(obs)][NO]$. As discussed in section 4, this shifted peak of $P(O_3)$ might imply a potential bias that the OBM tends to predict VOC-sensitive chemistry by daily integrated RIRs. However, the uncertainties of the daily integrated RIRs deriving from the possible errors of the diagnosed $P(O_3)$ would be smaller on VOC-sensitive days. This is because on the VOC-sensitive days, VOC-sensitive chemistry prevailed for the entire day, and the uncertainty of the calculated RIRs due to the diurnal variation of the modeled $P(O_3)$ should be small. On NO_x-sensitive days, the morning-to-afternoon evolution of the O_3 production regime was significant; hence the uncertainty of the calculated RIRs could be considerable.

[47] Besides the diagnosed results, correspondingly large differences in the k_{TVOC}/NO diurnal profile between NO_x- and VOC-sensitive days also occurred at both sites, and the variability seemed to be due mainly to diurnal variations in the NO concentration (Figure 11d). According to the diurnal patterns at the two sites, the ratio k_{TVOC}/NO matched the transition regime at about 4 s^{-1} ppb^{-1} or more, and the corresponding NO concentrations were about 1 ppbv or less. In addition, at the YUFA site, the afternoon NO concentrations that led to a high k_{TVOC}/NO ratio were about 100–200 pptv on NO_x-sensitive days and 500 pptv on VOC-sensitive days. At the PKU site, the afternoon NO concentrations were about 500 pptv on NO_x-sensitive days and 1500 pptv on VOC-sensitive days. On NO_x-sensitive days, the level of NO at below parts per billion by volume was sustained for one third to one half of the entire daytime hours at both sites. Therefore it can be seen that high-precision and accurate measurements of NO concentration are critical for correctly diagnosing the O_3-precursor relationships [*Cardelino and Chameides*, 2000]. Unfortunately, routine environmental monitoring stations in Beijing and elsewhere usually do not have the required precision.

6. Summary and Conclusions

[48] The comprehensive data set obtained in Beijing in summer 2006 provides us with a good opportunity for studying oxidant (O_3 + NO_2) production processes and formation regimes in Beijing. In situ observations of actinic flux, NO_x, O_3, VOCs, HONO, CO, OH, HO_2, H_2O_2, HNO_3, and wind direction and velocity were used to diagnose the $P(O_3)$-NO_x-VOC sensitivity. The daytime photochemical conditions were characterized by medium or low NO_x concentration and medium $j(O^1D)$ values combined with relatively high VOC reactivity and CO, O_3, and HONO concentrations. The urban site PKU consistently exhibited greater concentrations of all the O_3 precursors and a greater VOC reactivity than the suburban site YUFA.

[49] Influenced by the Asian monsoon and the valley winds condition, the southerly and northerly directions were the dominant wind directions. In both wind directions, modeled $P(O_3)$, which was consistent with the LIF measurements of HO_2 and k_{OH}, was much greater than the accumulation rate of the measured O_3 + NO_2 concentration. The high HONO concentration that was not supported by the current gas-phase mechanism was found to be a major cause for the high calculated $P(O_3)$.

[50] The oxidant formation regimes were diagnosed by OBM-derived daily integrated RIR values, instantaneous RIR* values, and the parameter L_N/Q. The daily integrated RIRs provide useful information for making reduction pol-

icies that target the attainment of 8 h at the air quality standard of O_3. The variation in RIRs demonstrated that both NO_x-sensitive and VOC-sensitive chemistry existed frequently at the two sites. However, at the PKU site, high-O_3 days were mostly characterized by a NO_x-sensitive condition. The variations in the O_3-sensitive chemistry were relatively well explained by the ratio of the average daytime k_{TVOC} and NO, with the transition chemistry corresponding to a k_{TVOC}/NO value of 2–4 s^{-1} ppb^{-1}. Results deduced from RIRs were tested by the afternoon average H_2O_2/HNO_3 derived from measurements. Relatively poor agreement was found between these two methods because the measured H_2O_2 was strongly influenced by factors other than the termination processes of HO_2. The important VOC groups for O_3 production were found to be alkenes, isoprene, and aldehydes for the YUFA site and alkenes, isoprene, aromatics, alkanes, and aldehydes for the PKU site. CO was also found to contribute a significant amount to OH reactivity at the two sites.

[51] The dependence of $P(O_3)$ on O_3 precursors was further diagnosed by comparing to the OBM-derived parameters L_N/Q and RIR*. In chemical coordinates of NO_x and VOC reactivity, all the samples were found to be partially sensitive to NO_x and partially sensitive to VOCs for both sites, which was also the case for the high-$P(O_3)$ samples. Over the mean diurnal profiles, pronounced diurnal variations in the O_3 production regime were found. In the morning, conditions were always strongly VOC-limited, while in the afternoon, conditions were variable for different days and different sites.

[52] The k_{TVOC}/NO dependence and the diurnal variations of the modeled $P(O_3)$ (or its proxy $k[HO_2(mod)][NO]$) and the model-derived L_N/Q for diagnosing the O_3 formation regime were compared to the corresponding values calculated from direct HO_x measurements by LIF. This comparison showed that the model might have a tendency to overpredict conditions of VOC-sensitive chemistry. However, since the chemical coupling between RO_2 and HO_2 is complicated [*Thornton et al.*, 2002], the tendency described above is not well understood because RO_2 radical measurements were not available.

[53] **Acknowledgments.** This work was supported by the National Natural Science Foundation of China (no. 40675072), the Ministry of Science and Technology of China (2002CB410801), and the Beijing Council of Science and Technology (HB200504-6 and no. HB200504-2). The authors would like to thank the CareBeijing-2006 team, especially M. Hu, L. M. Zeng, Z. M. Chen, F. Holland, Y. F. Cheng, X. Li, and S. R. Lou, for technical help and support at the field sites and F. Rohrer for help in IDL programming. We are grateful to the anonymous reviewers for their helpful comments on the manuscript.

References

Alicke, B., et al. (2003), OH formation by HONO photolysis during the BERLIOZ experiment, *J. Geophys. Res.*, *108*(D4), 8247, doi:10.1029/2001JD000579.

Atkinson, R., D. L. Baulch, R. A. Cox, J. N. Crowley, R. F. Hampson, J. A. Kerr, M. J. Rossi, and J. Troe (2001), Summary of evaluated kinetic and photochemical data for atmospheric chemistry, Int. Union of Pure and Appl. Chem. Subcom. on Gas Kinetic Data Eval. for Atmos. Chem., Research Triangle Park, N. C.

Bohn, B., et al. (2008), Photolysis frequency measurement techniques: Results of a comparison within the ACCENT project, *Atmos. Chem. Phys.*, *8*, 5373–5391.

Cardelino, C. A., and W. L. Chameides (1995), An observation-based model for analyzing ozone precursor relationships in the urban atmosphere, *J. Air Waste Manage. Assoc.*, *45*(3), 161–180.

Cardelino, C. A., and W. L. Chameides (2000), The application of data from photochemical assessment monitoring stations to the observation-based model, *Atmos. Environ.*, *34*, 2325–2332, doi:10.1016/S1352-2310(99)00469-0.

Carter, W. P. L., and R. Atkinson (1987), An experimental study of incremental hydrocarbon reactivity, *Environ. Sci. Technol.*, *21*(7), 670–679, doi:10.1021/es00161a008.

Chang, C. C., T. Y. Chen, C. Y. Lin, C. S. Yuan, and S. C. Liu (2005), Effects of reactive hydrocarbons on ozone formation in southern Taiwan, *Atmos. Environ.*, *39*, 2867–2878, doi:10.1016/j.atmosenv.2004.12.042.

Chen, T. F., and K. H. Chang (2006), Formulating the relationship between ozone pollution features and the transition value of photochemical indicators, *Atmos. Environ.*, *40*, 1816–1827, doi:10.1016/j.atmosenv.2005.11.025.

Daum, P. H., et al. (2004), Origin and properties of plumes of high ozone observed during the Texas 2000 Air Quality Study (TexAQS 2000), *J. Geophys. Res.*, *109*, D17306, doi:10.1029/2003JD004311.

Dodge, M. C. (2000), Chemical oxidant mechanisms for air quality modeling: Critical review, *Atmos. Environ.*, *34*, 2103–2130, doi:10.1016/S1352-2310(99)00461-6.

Edwards, G. D., et al. (2003), Chemical ionization mass spectrometer instrument for the measurement of tropospheric HO_2 and RO_2, *Anal. Chem.*, *75*(20), 5317–5327, doi:10.1021/ac034402b.

Gery, M. W., et al. (1989), A photochemical kinetics mechanism for urban and regional scale computer modeling, *J. Geophys. Res.*, *94*(D10), 12,925–12,956, doi:10.1029/JD094iD10p12925.

Heard, D. E., and M. J. Pilling (2003), Measurement of OH and HO_2 in the troposphere, *Chem. Rev.*, *103*(12), 5163–5198, doi:10.1021/cr020522s.

Hidy, G. M. (2000), Ozone process insights from field experiments. Part I: Overview, *Atmos. Environ.*, *34*, 2001–2022, doi:10.1016/S1352-2310(99)00456-2.

Hogo, H., and M. W. Gery (1988), *User's Guide for Executing OZIPM-4 (Ozone Isopleth Plotting With Optional Mechanisms, Version 4) With CBM-IV (Carbon-Bond Mechanisms-IV) or Optional Mechanisms*, U.S. Environ. Prot. Agency, Washington, D. C.

Holland, F., et al. (2003), Measurements of OH and HO_2 radical concentrations and photolysis frequencies during BERLIOZ, *J. Geophys. Res.*, *108*(D4), 8246, doi:10.1029/2001JD001393.

Hua, W., et al. (2008), Atmospheric hydrogen peroxide and organic hydroperoxides during PRIDE-PRD'06, China: Their concentration, formation mechanism and contribution to secondary aerosols, Atmos. *Chem. Phys. Discuss.*, *8*(3), 10,481–10,530.

Kanaya, Y., et al. (2008), Urban photochemistry in central Tokyo: 2. Rates and regimes of oxidant (O_3 + NO_2) production, *J. Geophys. Res.*, *113*, D06301, doi:10.1029/2007JD008671.

Kleffmann, J. (2007), Daytime sources of nitrous acid (HONO) in the atmospheric boundary layer, *Chem. Phys. Chem.*, *8*(8), 1137–1144, doi:10.1002/cphc.200700016.

Kleffmann, J., et al. (2002), A new instrument (LOPAP) for the detection of nitrous acid (HONO), *Environ. Sci. Pollut. Res.*, *9*(4), 48–54.

Kleffmann, J., et al. (2005), Daytime formation of nitrous acid: A major source of OH radicals in a forest, *Geophys. Res. Lett.*, *32*, L05818, doi:10.1029/2005GL022524.

Kleinman, L. I. (2000), Ozone process insights from field experiments. Part II: Observation-based analysis for ozone production, *Atmos. Environ.*, *34*, 2023–2033, doi:10.1016/S1352-2310(99)00457-4.

Kleinman, L. I. (2005), The dependence of tropospheric ozone production rate on ozone precursors, *Atmos. Environ.*, *39*, 575–586, doi:10.1016/j.atmosenv.2004.08.047.

Kleinman, L. I., et al. (1997), Dependence of ozone production on NO and hydrocarbons in the troposphere, *Geophys. Res. Lett.*, *24*(18), 2299–2302, doi:10.1029/97GL02279.

Kleinman, L. I., et al. (2001), Sensitivity of ozone production rate to ozone precursors, *Geophys. Res. Lett.*, *28*(15), 2903–2906, doi:10.1029/2000GL012597.

Kleinman, L. I., et al. (2002), Ozone production efficiency in an urban area, *J. Geophys. Res.*, *107*(D23), 4733, doi:10.1029/2002JD002529.

Kleinman, L. I., et al. (2005), A comparative study of ozone production in five U.S. metropolitan areas, *J. Geophys. Res.*, *110*, D02301, doi:10.1029/2004JD005096.

Levy, H., et al. (1985), Tropospheric ozone: The role of transport, *J. Geophys. Res.*, *90*(D2), 3753–3772, doi:10.1029/JD090iD02p03753.

Liu, S. C. (1977), Possible effects on tropospheric O_3 and OH due to NO emissions, *Geophys. Res. Lett.*, *4*(8), 325–328, doi:10.1029/GL004i008p00325.

Martinez, M., et al. (2003), OH and HO_2 concentrations, sources, and loss rates during the southern oxidants study in Nashville, Tennessee, summer 1999, *J. Geophys. Res.*, *108*(D19), 4617, doi:10.1029/2003JD003551.

Mihelcic, D., et al. (2003), Peroxy radicals during BERLIOZ at Pabstthum: Measurements, radical budgets and ozone production, *J. Geophys. Res.*, *108*(D4), 8254, doi:10.1029/2001JD001014.

North American Research Strategy for Tropospheric Ozone (2000), *An Assessment of Tropospheric Ozone Pollution: A North American Perspective*, North Am. Res. Strategy for Tropospheric Ozone Manage. Off. (Envair), Pasco, Wash.

Ren, X. R., et al. (2003), OH and HO_2 chemistry in the urban atmosphere of New York City, *Atmos. Environ.*, *37*, 3639–3651, doi:10.1016/S1352-2310(03)00459-X.

Richter, A., et al. (2005), Increase in tropospheric nitrogen dioxide over China observed from space, *Nature*, *437*(7055), 129–132, doi:10.1038/nature04092.

Ryerson, T. B., et al. (2003), Effect of petrochemical industrial emissions of reactive alkenes and NO_x on tropospheric ozone formation in Houston, Texas, *J. Geophys. Res.*, *108*(D8), 4249, doi:10.1029/2002JD003070.

Sadanaga, Y., et al. (2004), Development of a measurement system of OH reactivity in the atmosphere by using a laser-induced pump and probe technique, *Rev. Sci. Instrum.*, *75*(8), 2648–2655, doi:10.1063/1.1775311.

Shao, M., et al. (2005), Major reactive species of ambient volatile organic compounds (VOCs) and their sources in Beijing, *Sci. China Ser. D Earth Sci.*, *48*(Suppl. II), 147–154, doi:10.1360/05yd0398.

Shao, M., et al. (2006), City clusters in China: Air and surface water pollution, *Front. Ecol. Environ.*, *4*, 353–361, doi:10.1890/1540-9295(2006)004[0353:CCICAA]2.0.CO;2.

Shirley, T. R., et al. (2006), Atmospheric oxidation in the Mexico City Metropolitan Area (MCMA) during April 2003, *Atmos. Chem. Phys.*, *6*, 2753–2765.

Shiu, C. J., et al. (2007), Photochemical production of ozone and control strategy for southern Taiwan, *Atmos. Environ.*, *41*, 9324–9340, doi:10.1016/j.atmosenv.2007.09.014.

Sillman, S. (1995), The use of NOy, H_2O_2, and HNO_3 as indicators for ozone-NO_x-hydrocarbon sensitivity in urban locations, *J. Geophys. Res.*, *100*(D7), 14,175–14,188, doi:10.1029/94JD02953.

Sillman, S. (1999) The relation between ozone, NO_x and hydrocarbons in urban and polluted rural environments, *Atmos. Environ.*, *33*, 1821–1845, doi:10.1016/S1352-2310(98)00345-8.

Sillman, S., and D. Y. He (2002), Some theoretical results concerning O_3-NO_x-VOC chemistry and NO_x-VOC indicators, *J. Geophys. Res.*, *107*(22), 4659, doi:10.1029/2001JD001123.

Sillman, S., et al. (1990), The sensitivity of ozone to nitrogen oxides and hydrocarbons in regional ozone episodes, *J. Geophys. Res.*, *95*(D2), 1837–1851, doi:10.1029/JD095iD02p01837.

Solomon, P., et al. (2000), Comparison of scientific findings from major ozone field studies in North America and Europe, *Atmos. Environ.*, *34*, 1885–1920, doi:10.1016/S1352-2310(99)00453-7.

Song, Y., et al. (2007), Source apportionment of ambient volatile organic compounds in Beijing, *Environ. Sci. Technol.*, *41*(12), 4348–4353, doi:10.1021/es0625982.

Stemmler, K., et al. (2006), Photosensitized reduction of nitrogen dioxide on humic acid as a source of nitrous acid, *Nature*, *440*(7081), 195–198, doi:10.1038/nature04603.

Su, H., et al. (2008a), Observation of nighttime nitrous acid (HONO) formation at a non-urban site during PRIDE-PRD2004 in China, *Atmos. Environ.*, *42*, 6219–6232, doi:10.1016/j.atmosenv.2008.04.006.

Su, H., et al. (2008b), Nitrous acid (HONO) and its daytime sources at a rural site during the 2004 PRIDE-PRD experiment in China, *J. Geophys. Res.*, *113*, D14312, doi:10.1029/2007JD009060.

Tang, X., et al. (1990), Atmospheric Environmental Chemistry, 1st ed., Higher Educ. Press, Beijing, China.

Thornton, J. A., et al. (2002), Ozone production rates as a function of NO_x abundances and HO_x production rates in the Nashville urban plume, *J. Geophys. Res.*, *107*(D12), 4146, doi:10.1029/2001JD000932.

Volz-Thomas, A., et al. (2003), Inorganic trace gases and peroxy radicals during BERLIOZ at Pabstthum: An investigation of the photostationary state of NO_x and O_3, *J. Geophys. Res.*, *108*(D4), 8248, doi:10.1029/2001JD001255.

Wang, J. L., et al. (2008), Characterization of ozone precursors in the Pearl River Delta by time series observation of non-methane hydrocarbons, *Atmos. Environ.*, *42*, 6233–6246, doi:10.1016/j.atmosenv.2008.01.050.

Wang, T., et al. (2006), Strong ozone production in urban plumes from Beijing, China, Geophys. *Geophys. Res. Lett.*, *33*, L21806, doi:10.1029/2006GL027689.

Xie, X., et al. (2008), Estimate of initial isoprene contribution to ozone formation potential in Beijing, China, *Atmos. Environ.*, *42*, 6000–6010, doi:10.1016/j.atmosenv.2008.03.035.

Zhang, J., et al. (2007), Ozone production and hydrocarbon reactivity in Hong Kong, southern China, *Atmos. Chem. Phys.*, *7*, 557–573.

Zhang, Y., et al. (1998), Photochemical pollution in Chinese cities, *Acta Sci. Nat. Univ. Pekinensis*, *34*(2–3), 392–400.

Zhang, Y. H., et al. (2008a), Regional integrated experiments on air quality over Pearl River Delta 2004 (PRIDE-PRD2004): Overview, *Atmos. Environ.*, *42*, 6157–6173, doi:10.1016/j.atmosenv.2008.03.025.

Zhang, Y. H., et al. (2008b), Regional ozone pollution and observation-based approach for analyzing ozone-precursor relationship during the PRIDE-PRD2004 campaign, *Atmos. Environ.*, *42*, 6203–6218, doi:10.1016/j.atmosenv.2008.05.002.

T. Brauers, A. Hofzumahaus, and A. Wahner, Institute ICG-II: Troposphere, Forschungszentrum Jülich, D-52425 Jülich, Germany.

C. C. Chou and S. C. Liu, Research Center of Environment Change, Academia Sinica, 128 Academia Rd., Section 2, Nankang, Taipei 115, Taiwan.

K. Kita, Faculty of Science, Ibaraki University, 2-1-1 Bunkyo, Mito, Ibaraki 310-8512, Japan.

Y. Kondo, Research Center for Advanced Science and Technology, University of Tokyo, Tokyo 153-8904, Japan.

K. Lu, M. Shao, H. Su, X. Wang, Y. Zhang (corresponding author), and T. Zhu, College of Environmental Sciences and Engineering, Peking University, Beijing 100871, China. (yhzhang@pku.edu.cn)

J. Wang, Department of Chemistry, National Central University, Chungli 320, Taiwan.